Molecular mechanism of hydromorphone preconditioning in cerebral ischemia/reperfusion-induced inflammatory injury

JING YAO, ZEQING HUANG, SONGZE LI, MINGHUI LUN and JIANING FAN

Department of Anesthesiology, Cancer Hospital of China Medical University, Liaoning Cancer Hospital and Institute, Cancer Hospital of Dalian University of Technology, Shenyang, Liaoning 110042, P.R. China

Received May 22, 2025; Accepted May 14, 2026

DOI: 10.3892/ijmm.2026.5895

Abstract. The present study explored the protective mechanism of hydromorphone (HM) preconditioning in cerebral ischemia/reperfusion injury (CIRI). An animal model of CIRI was established by middle cerebral artery occlusion/reperfusion in male C57BL/6J mice. An I/R cell model was induced by oxygen-glucose deprivation/reperfusion. Brain tissue injury and cell injury were evaluated by hematoxylin and eosin staining, 2,3,5-triphenyltetrazolium chloride staining, lactate dehydrogenase testing and a Cell Counting Kit-8 assay. Nod-like receptor protein 3 (NLRP3)-positive expression and caspase-1 activity were assessed by immunostaining and caspase-1 activity assays, respectively. Reverse transcription-quantitative PCR or western blotting were used to quantify the expression levels of microRNA (miR)-195-5p, RNA-binding motif protein 15 (RBM15) and upstream stimulatory factor 2 (USF2). RNA immunoprecipitation (RIP) and dual-luciferase assays verified the binding between miR-195-5p and RBM15, followed by RIP analysis of N6-methyladenosine (m6A) enrichment on USF2 and quantitative analysis of m6A content. The binding of RBM15 and insulin-like growth factor 2 mRNA-binding protein 3 (IGF2BP3) to the USF2 m6A site was analyzed by a dual-luciferase assay. HM preconditioning inhibited NLRP3-mediated pyroptosis, alleviated neurological deficits, and reduced inflammatory injury in brain tissue. Mechanistically, hydromorphone (HM) preconditioning targeted RBM15 and reduced IGF2BP3-mediated m6A modification by upregulating miR-195-5p expression, thus decreasing USF2 expression, reducing the enrichment of USF2 on the NLRP3 promoter, and inhibiting NLRP3-mediated pyroptosis. In conclusion, HM preconditioning may repress NLRP3-mediated pyroptosis and alleviate CIRI via the effects of miR-195-5p/RBM15/USF2.

Correspondence to: Ms. Jianing Fan, Department of Anesthesiology, Cancer Hospital of China Medical University, Liaoning Cancer Hospital and Institute, Cancer Hospital of Dalian University of Technology, 44 Xiaohe Yan Road, Dadong, Shenyang, Liaoning 110042, P.R. China
E-mail: fanjianing0410@163.com

Abbreviations: HM, hydromorphone; I/R, ischemia/reperfusion; CIRI, cerebral ischemia/reperfusion injury; RBM15, RNA-binding motif protein 15; USF2, upstream stimulatory factor 2; IGF2BP3, insulin-like growth factor 2 mRNA-binding protein 3; miRNA or miR, microRNA; m6A, N6-methyladenosine; MCAO/R, middle cerebral artery occlusion/reperfusion; OGD/R, oxygen-glucose deprivation/reperfusion; CBF, cerebral blood flow; ORs, opioid receptors; Nig, nigericin; HBMVECs, human brain microvascular endothelial cells; H&E, hematoxylin and eosin; TTC, 2,3,5-triphenyltetrazolium chloride; ELISA, enzyme-linked immunosorbent assay; IL, interleukin; TNF-α, tumor necrosis factor alpha; DMEM, Dulbecco's modified Eagle's medium; NLRP3, nod-like receptor protein 3; FBS, fetal bovine serum; PBS, phosphate-buffered saline; CCK-8, Cell Counting Kit-8; LDH, lactate dehydrogenase; CPK, creatine phosphokinase; RIP, RNA immunoprecipitation; ChIP, chromatin immunoprecipitation; RT-qPCR, reverse transcription-quantitative polymerase chain reaction; GAPDH, glyceraldehyde-3-phosphate dehydrogenase; ANOVA, analysis of variance

Key words: cerebral I/R, HM, miR-195-5p, RBM15, pyroptosis, USF2, NLRP3, IGF2BP3, m6A, transcription factor

Introduction

Ischemic stroke primarily results from cerebral artery occlusion, leading to insufficient glucose and oxygen in brain cells. Restoring blood flow perfusion is the main treatment strategy for ischemic stroke. Nevertheless, rapid reperfusion inevitably leads to secondary brain tissue injury, namely, cerebral ischemia/reperfusion injury (CIRI) (1,2). The pathological process of CIRI is complicated and involves the interaction of numerous factors, including the inflammatory response, oxidative stress, energy metabolism disorders and neuronal death (3). Pyroptosis is a recently discovered form of programmed cell death that mediates neuroinflammation after ischemic stroke, and the suppression of pyroptosis may hold substantial promise for rescuing neurological deterioration during CIRI (4,5). Owing to irreversible neuronal death, the prognosis of CIRI is dismal. Therefore, preventing and reducing neuronal death in CIRI remains a medical hotspot worthy of extensive research.

Opioid receptors (ORs), including mu ORs (MORs), delta ORs (DORs), and kappa ORs (KORs), exhibit both short- and long-term alterations and are redistributed in brain regions after ischemic stroke in rodents (6).

Appropriate activation of ORs at specific times and regions may be a crucial neuroprotective strategy after stroke (7,8). Opioid agents act by non-overlapping molecular mechanisms, including stimulating the release of neurotrophic factors, protecting cerebral vascular autoregulation, limiting glutamate release, reducing oxidative injury, and maintaining brain homeostasis to exert neuroprotective effects (9). Hydromorphone (HM), a potent opioid analgesic widely used for pain relief (10), has been reported to protect against ischemic oxidative stress in rat glial cells (11). HM preconditioning markedly represses I/R-induced neuronal apoptosis in the hippocampal CA1 region and alleviates oxidative stress (12). HM restrains Nod-like receptor protein 3 (NLRP3) inflammasome-mediated pyroptosis by activating the Nrf2/HO-1 pathway (13). Nevertheless, there is currently no relevant research reporting the effect of HM on pyroptosis in CIRI. In accordance with previous studies (14-16), human brain microvascular endothelial cells (HBMVECs) were chosen to establish an I/R cell model to investigate the effect of HM on cell pyroptosis.

microRNAs (miRNAs or miRs) are a class of small non-coding RNAs (~22 nucleotides in length) that play vital roles in CIRI (17). One such miRNA, miR-195-5p, has been shown to mitigate CIRI via PTEN-AKT signaling (16). A miR-195-5p inhibitor aggravated inflammation and apoptosis in oxygen-glucose deprivation/reperfusion (OGD/R)-induced cells (18). miR-195-5p expression is also notably reduced in mouse I/R testis tissues, and miR-195-5p represses testicular I/R-induced pyroptosis (19). The expression of miR-195-5p can be upregulated by the use of propofol, another commonly used anesthetic drug (20). However, whether HM can affect miR-195-5p expression remains unclear.

N6-methyladenosine (m6A) is the most prevalent RNA epigenetic modulator in eukaryotic cells and plays a pivotal role in physiological processes during CIRI (21). m6A modification is orchestrated by methyltransferases (writers), removed by demethylases (erasers), and recognized by RNA-binding proteins (readers) (22). RBM15 functions as a recruiter/adapter for the writer complex, and its expression is upregulated in ischemic stroke samples compared with controls (23). RNA-binding motif protein 15 (RBM15) intensifies inflammation, oxidative stress and pyroptosis to facilitate diabetic nephropathy progression (24). A binding relationship between miR-195-5p and RBM15 was predicted through the Starbase database (https://rnasysu.com/encori/). Hence, it was hypothesized that HM preconditioning affects pyroptosis in CIRI via miR-195-5p/RBM15. The present study aimed to investigate the underlying protective mechanism of HM preconditioning in CIRI, providing a theoretical basis for improving the prognosis of CIRI.

Materials and methods

Ethics statement. The study procedure was approved by the Ethics Committee of Liaoning Cancer Hospital and Institute (approval no. CMU20250031; Shenyang; China). All animal experimental procedures were approved by the Animal Ethics Committee of Liaoning Cancer Hospital and Institute and implemented on the basis of the Guide for the Care and Use of Laboratory Animals (25).

Database prediction. The downstream target genes of miR-195-5p were predicted using the Starbase database (https://rnasysu.com/encori/) (26), and the binding site between miR-195-5p and RBM15 was determined. The m6A modification level of USF2 was predicted using the SRAMP database (http://www.cuilab.cn/sramp/) (27). The binding between USF2 and NLRP3 was predicted using the JASPAR database (http://jaspar.genereg.net/) (28).

Establishment and treatment of a mouse I/R model. Male C57BL/6J mice (7-8 weeks; 20-25 g) were purchased from Vital River Laboratory Animal Technology Co., Ltd. and kept under specific pathogen-free conditions at 21-24˚C with a light/dark cycle of 12/12-h. Mice had free access to water and food (both sterilized). The water bottles and padding were regularly replaced, and the cages were disinfected.

After they were weighed, the mice were grouped according to random numbers, which were recorded by surgical personnel. The mice were randomly divided into 6 groups [9 mice per group, calculated by G * Power, Effect size: f=0.6, α err prob=0.05, and Power (1-β err prob)=0.9]. In the sham group, mice underwent all the same surgical procedures as the I/R group mice, except that the arteries were not ligated; I/R group: mice with ischemia for 30 min; I/R + saline group: mice with subcutaneous injection of 0.9% physiological saline for 5 days, followed by 30 min of ischemia; I/R + HM group: mice with subcutaneous injection of 2 mg/kg HM (Yichang Humanwell Pharmaceutical Co., Ltd.; NMPN: H20120100; cat. no. TD2012-0010) for 4 consecutive days and injection of 3 mg/kg HM 4 h before surgery (12), followed by 30 min of ischemia. In the I/R + HM + antagomir NC group, mice were subcutaneously injected with 2 mg/kg HM for 4 consecutive days, 100 μM antagomir NC was injected into the mouse ventricle stereotactically one day before surgery, and another 3 mg/kg HM was injected 4 h before surgery, followed by 30 min of ischemia; in the I/R + HM + antagomir-195 group, mice were subcutaneously injected with 2 mg/kg HM for 4 consecutive days, 100 μM antagomir-195 was injected into the mouse ventricle stereotactically one day before surgery, and another 3 mg/kg HM was injected 4 h before surgery, followed by 30 min of ischemia. The specific experimental process is shown in Fig. 1. The miR-195-5p antagomir (antagomir-195) and antagomir-NC were purchased from Shanghai GenePharma Co., Ltd. Stereotactic coordinates: Anteroposterior, 0.8 mm; mediolateral, 1.5 mm; depth, 3.5 mm. The surgery was performed under anesthesia using a stereotaxic device (RWD Life Science). In total, 100 μM antagomir-NC or antagomir-195 was injected into the mouse ventricle via the stereotaxic method (16) at a rate of 0.5 μl/min. The needle was kept in its original position for 5 min and slowly withdrawn, after which the skin incision was sutured.

The mice were anaesthetized by intraperitoneal injection of pentobarbital sodium (30 mg/kg) 4 h after the last administration of HM (16), and the body temperature was maintained at 37±1.0˚C on a heating pad throughout all the experimental procedures. Afterwards, the junction of the carotid artery and the proximal end of the internal carotid artery was exposed through a midline incision in the neck under a surgical microscope. A 6-0 monofilament coated with silicone was inserted

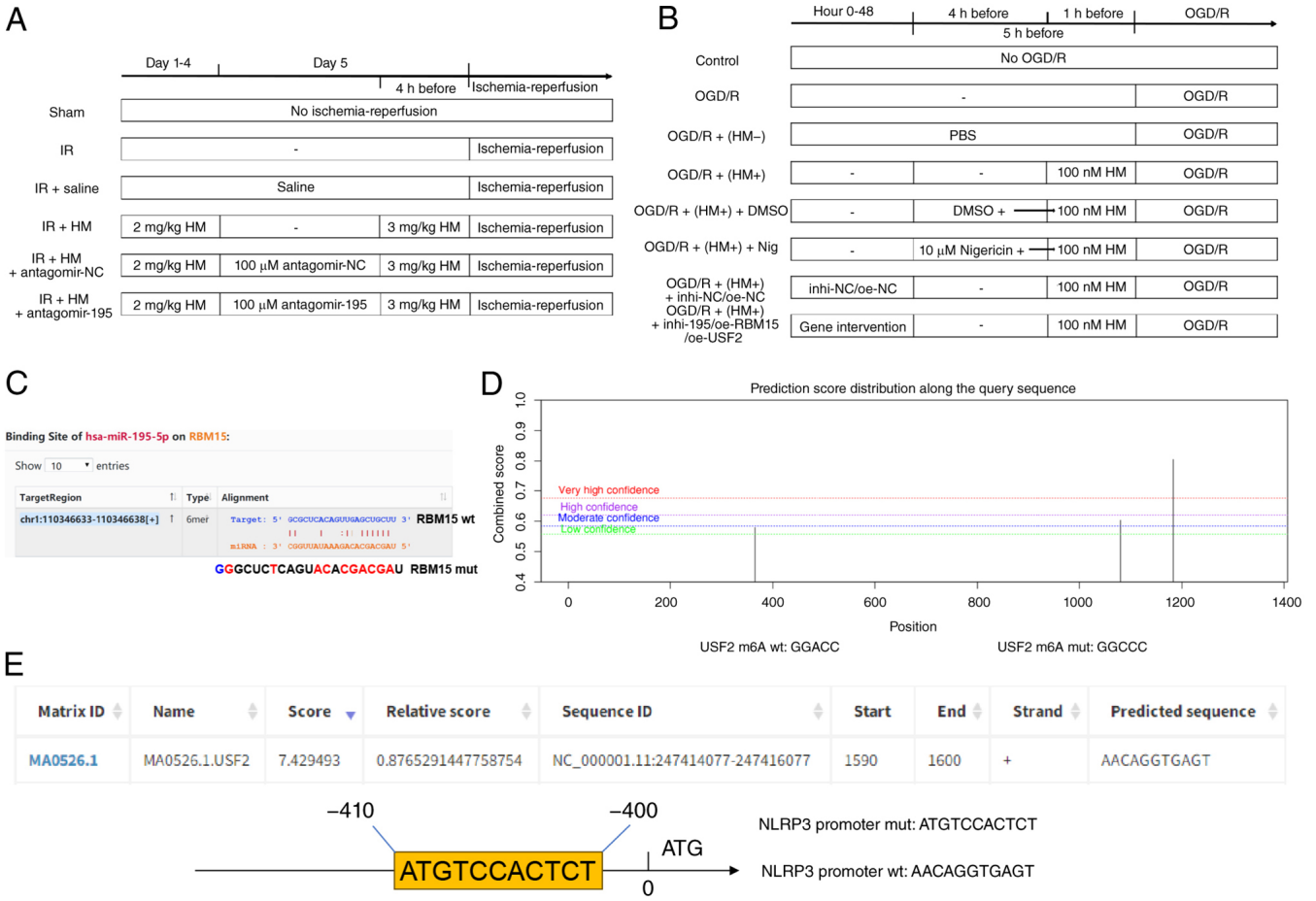

Figure 1. HM preconditioning flowchart and database prediction results. (A) Establishment and processing flow of the IR mouse model. (B) Establishment and processing flow of the OGD/R cell model. (C) Prediction of the binding site between miR-195-5p and RBM15 using the Starbase database. (D) Prediction of the m6A modification level of USF2 using the SRAMP database. (E) Prediction of the binding between USF2 and NLRP3 using the JASPAR database. HM, hydromorphone; I/R, ischemia/reperfusion; OGD/R, oxygen-glucose deprivation/reperfusion; m6A, N6-methyladenosine; USF2, upstream stimulatory factor 2; NLRP3, Nod-like receptor protein 3; NC, negative control; WT, wild-type; MUT, mutant; miR, microRNA.

into the carotid artery at a distance of 7±0.5 mm below the carotid branch until mild resistance was felt (29). After 30 min of ischemia, the monofilament was removed to achieve reperfusion. Blood flow was observed using a laser Doppler perfusion imaging device (PeriCam PSI HR; https://www.perimed-instruments.com/). A decrease of more than 30% in cerebral blood flow (CBF) relative to baseline was considered sufficient induction of ischemia. After the obstructive filament was removed, an increase in the CBF to more than 70% of the baseline value was considered successful reperfusion. All the animals were operated on by the same operator under the same conditions to reduce the variability of infarction. The surgery time for each animal did not exceed 15 min. After 24 h, the neurological deficits of the mice were assessed. To evaluate brain injury, 0.5 ml of blood was collected from the orbital vein of each mouse, and serum was collected after centrifugation (2,000 x g, 4˚C, 15 min). Finally, the mice were euthanized by intraperitoneal injection of sodium pentobarbital (200 mg/kg). Death was confirmed by observing respiratory arrest, disappearance of nerve reflex and muscle relaxation, in combination with observation of heartbeat (touching the apical beat). The brain tissues were collected for subsequent experiments. During the experiment, if the mice were unable to independently drink water, experienced severe breathing difficulties and cyanosis, and were unable to stand, euthanasia was immediately carried out.

Assessment of neurological deficits. In most literature on cerebral ischemia-reperfusion (30-36), Longa score is used to evaluate neurological deficits. In the present study, neurofunctional deficits were assessed using the slightly modified Longa score as previously described (16,37): 0, no neurological deficit; 1, the contralateral front paws cannot fully extend; 2, mice have difficulty turning to the opposite side; 3, mice cannot turn to the opposite side; and 4, mice are unable to walk independently and have decreased consciousness. The scoring was blindly conducted by two independent observers.

2,3,5-Triphenyltetrazolium chloride (TTC) staining. TTC staining was used to evaluate the infarct volume in mice after reperfusion. The brain tissues were cut into 2-mm sections and cultured in 2% TTC solution (cat. no. 17779; Sigma-Aldrich; Merck KGaA) at 37˚C for 20 min. Then, the sections were fixed with 4% paraformaldehyde (cat. no. P0099-3L; Beyotime Institute of Biotechnology) for 2 h and images were captured with a digital camera. Unstained white areas were considered infarct areas, and stained red areas were considered non-infarct areas. The infarct volume was analyzed by

Image-Pro Plus 6.0 (Media Cybernetics, Inc.). The infarct volume was calculated by summing the infarct areas of all the sections and multiplying them by the section thickness. To consider possible oedema, the following formula (38) was used to quantify the infarct volume (%) after oedema correction: [(contrasting hemisphere volume-non-infarct area volume of aqueous hemisphere)/contrasting hemisphere volume] x100%. The measurements were conducted blindly by two separate observers.

Hematoxylin and eosin (H&E) staining. H&E staining (cat. no. C0105M; Beyotime Institute of Biotechnology) was used to evaluate mouse brain histopathological injury (39). After reperfusion, the brain tissue (cortical area) samples were fixed overnight in 4% paraformaldehyde at 4˚C and embedded in paraffin. Afterwards, the brain tissues were cut into 5-μm sections, deparaffinized using xylene (cat. no. 016371.M1; Thermo Fisher Scientific, Inc.) twice, with each treatment lasting 5-10 min, and rehydrated with gradient ethanol. Afterwards, the tissues were stained with hematoxylin for 5 min, incubated with acetic acid for 1 min, stained with eosin for 1 min, and dehydrated with gradient ethanol. Finally, the tissues were sealed with neutral resin and images were captured under a light microscope.

Cell culture and establishment of OGD/R cells. As human derived cells are more closely related to the clinical pathological environment, HBMVECs were selected as the main cells by referring to previous studies (14-16,40-43). HBMVECs (RRID: CVCL_4D10) (https://www.atcc.org/products/crl-3245) were obtained from American Type Culture Collection (cat. no. CRL-3245) and cultured in Dulbecco's modified Eagle's medium (DMEM) supplemented with 10% fetal bovine serum (FBS; cat. no. C0237; Beyotime Institute of Biotechnology) at 37˚C with 5% CO_2. The culture medium was changed every 3 days, and cells at the 3rd to 6th passages were used in the present study. The cells were validated by short tandem repeats and tested negative for mycoplasma. To simulate cerebral I/R *in vivo*, as previously described (16), the cells were subjected to OGD/R. In brief, the cells were exposed to glucose-free DMEM and cultured at 37˚C with 95% N_2/5% CO_2 for 2 h. Then, the glucose-free DMEM was replaced with DMEM containing glucose, and the cells were cultured in a normal state for 24 h for reoxidation. The control cells were cultured under normal conditions.

Cell treatment. The miR-195-5p inhibitor (inhi-195) and corresponding NC (inhi-NC) were synthesized by Guangzhou RiboBio Co., Ltd. To overexpress RBM15 (accession no. NM_001201545), IGF2BP3 (accession no. NM_006547), and USF2 (accession no. NM_001321150), their full length was cloned and they were inserted into the vector pcDNA3.1 (Shanghai GeneChem Co., Ltd.) to generate the overexpression plasmids oe-RBM15, oe-IGF2BP3 and oe-USF2, with the empty vector pcDNA3.1 (oe-NC) as a negative control. Small interfering (si)RNAs targeting *IGF2BP3* (si-IGF2BP3) and its NC (si-NC) were purchased from Guangzhou RiboBio Co., Ltd. Then, transfection was performed using Lipofectamine 3000 (Invitrogen; Thermo Fisher Scientific, Inc.). After 48 h of transfection. For each transfection, 50 nmol/l of RNA duplexes were used. The transfection efficiency was validated using reverse transcription-quantitative PCR (RT-qPCR). To determine the dosage of HM, a preliminary experiment was conducted. The cells were treated with three different doses (10, 100, or 1,000 nM) of HM for 1 h (11), followed by OGD/R. For NLRP3 agonist treatment, OGD/R was performed after 5 h of treatment with 10 μM nigericin (Nig) (44). The relevant sequences are shown in Table SI.

Cell Counting Kit-8 (CCK-8) assay. The cells ($1x10^4$) were seeded into a 96-well plate and cultured for 24 h (16). Afterwards, 10 μl of CCK-8 solution (cat. no. 96992; MilliporeSigma) was added to each well, and the cells were incubated at 37˚C for another 2 h. The optical density at 450 nm was measured using a microplate reader (BioTek; Agilent Technologies, Inc.).

Caspase-1 activity assay. Caspase-1 enzyme activity was measured using a caspase-1 fluorescence assay kit (cat. no. ab39412; Abcam) (45). Cells were cultured in the corresponding manner, collected, and processed according to the assay protocol. The cell suspension was resuspended in lysis buffer and centrifuged (3,000 x g, 4˚C, 5 min). Afterwards the supernatant was collected. The sample wells and background wells were set in black 96-well cell culture plates with clear bottoms. Afterwards, the reaction mixture was prepared and added to each well along with the fluorescent label, followed by incubation at 37˚C for 1-2 h. Finally, the fluorescence output was measured by a plate reader.

Lactate dehydrogenase (LDH) release. Serum LDH levels in mice were detected using an LDH assay kit (cat. no. C0016; Beyotime Institute of Biotechnology) (39). In brief, the cells were seeded into 96-well plates ($3x10^4$ cells/well) (18) and washed once with phosphate-buffered saline (PBS) (cat. no. C0221A; Beyotime Institute of Biotechnology) after the culture medium was removed. Afterwards, 400 g of cell culture plate was removed and centrifuged for 5 min. The supernatant (120 μl) was added to each well of a new 96-well plate supplemented with 60 μl of LDH detection solution and incubated at 37˚C for 30 min. The absorbance at 490 nm was measured using a microplate reader.

Immunofluorescence staining of NLRP3. After they were incubated with 0.3% Triton X-100 and 10% bovine serum albumin (BSA; cat. no. ST2254; Beyotime Institute of Biotechnology) for 1 h (46), the brain tissue (cortical area) sections were fixed with 4% paraformaldehyde, infiltrated with 0.2% Triton X-100 for 10 min, and blocked with 5% BSA at room temperature for 90 min (47). Afterwards, the cells were incubated overnight with rabbit anti-NLRP3 (1:100; RRID: AB_2809541; cat. no. MA5-32255; Thermo Fisher Scientific, Inc.) at 4˚C and the corresponding goat anti-rabbit IgG H&L (Alexa Fluor® 488; cat. no. ab150077; Abcam) at room temperature for 2 h. DAPI (1 μg/ml) was used to stain the cell nucleus. The images were captured under a fluorescence microscope (BioTek; Agilent Technologies, Inc.).

Enzyme-linked immunosorbent assay (ELISA). After reperfusion, the brain tissues were ice sealed with physiological saline and frozen at -20˚C for 5 min. Then, the brain tissues were centrifuged at 800 x g for 15 min to obtain the supernatant.

Table I. Primer sequences.

Gene name	Primer sequence (5'-3')	Efficiency (%)
Mouse		
miR-195-5p	F: GCGCGATAGCAGCACAGAAAT	101
	R: GTGTCGTGGAGTCGGCAATTC	
RBM15	F: TGCCAACCGGACACTTTTCT	107
	R: GCCATAGGTACTGGTCTGGC	
USF2	F: GTAGTCCAGGTGACTGATGGT	109
	R: GGATTTTGAATTACAGCCTGGGT	
NLRP3	F: GACCGTGAGGAAAGGACCAG	109
	R: GGCCAAAGAGGAATCGGACA	
GAPDH	F: AGGTTCATCAGGTAAACTCAGG	107
	R: TTGATGGCAACAATCTCCACT	
U6	F: CGCTTCGGCAGCACATATACT	100
	R: CTTCACGAATTTGCGTGTCAT	
Human		
miR-195-5p	F: GGCGTAGGTAGCAGCACAGAA	108
	R: CTCAACTGGTGTCGTGGAGTC	
RBM15	F: GCCTTCCCACCTTGTGAGTT	107
	R: TCAACCAGTTTTGCACGGAC	
USF2	F: ACAAATGGAGGACAGACAGGA	107
	R: CCTCTCATCTCGGGGTGTTC	
IGF2BP3	F: CTGCACGGGAAACCCATAGA	103
	R: TCCCACTGTAAATGAGGCGG	
NLRP3	F: AGAAGCTCTGGTTGGTCAGC	100
	R: CAAGGCATTCTCCCCCACAT	
NLRP3 promoter	F: GCCTGCCACATACCAGCCATT	96
	R: GTCCTCTCACAGCAAGATGGCT	
GAPDH	F: GTCAAGGCTGAGAACGGGAA	100
	R: TCGCCCCACTTGATTTTGGA	
U6	F: CTCGCTTCGGCAGCACATATA	103
	R: TGGAACGCTTCACGAATTTGC	

F, forward; R, reverse; miR, microRNA; RBM15, RNA-binding motif protein 15; USF2, upstream stimulatory factor 2; NLRP3, Nod-like receptor protein 3; IGF2BP3, insulin-like growth factor 2 mRNA-binding protein 3.

In the cell experiments, cells were isolated from the culture medium and then centrifuged at 3,000 x g for 30 min to obtain the supernatant (42). To determine the release of S100B (48,49), inflammatory cytokines and pyroptosis factors, mouse serum, brain tissue homogenate and cell culture supernatant were collected, and the concentrations of S100B (cat. no. ab285283), TNF-α (cat. nos. ab208348/ab181421), IL-6 (cat. nos. ab222503/ab178013), IL-4 (cat. nos. ab215089/ab100710), IL-10 (cat. nos. ab255729/ab185986), IL-1β (cat. nos. ab197742/ab214025) and IL-18 (cat. nos. ab216165/ab215539) were measured using ELISA kits (Abcam). The absorbance at 450 nm was measured using a microplate reader.

RT-qPCR. Total RNA was extracted from brain tissues or cells using TRIzol reagent (cat. no. 15596026CN; Invitrogen; Thermo Fisher Scientific, Inc.). RT-qPCR was performed to detect gene expression. A FastQuant RT assay kit (Tiangen Biotech Co., Ltd.) was used to synthesize complementary DNA (cDNA) according to the manufacturer's instructions. RT-qPCR was performed on a real-time thermal cycler (Applied Biosystems; Thermo Fisher Scientific, Inc.) and using a SYBR Green I fluorescence kit (Takara Biotechnology Co., Ltd.). The amplification mixture included 20 μl: 10 μl of SYBR Green mix, 0.4 μl of forward primer, 0.4 μl of reverse primer, 3 μl of cDNA, and 6.2 μl of RNase-free water. The reaction conditions were as follows: 95˚C for 30 sec, 95˚C for 15 sec, and 60˚C for 30 sec for 40 cycles. The primer sequences are shown in Table I. With glyceraldehyde-3-phosphate dehydrogenase (GAPDH) and U6 (18) as internal reference genes, the fold difference in gene expression was calculated via the $2^{-\Delta\Delta Cq}$ method (50).

Western blotting. The protein was extracted using radioimmunoprecipitation assay (RIPA) buffer (cat. no. P0013B; Beyotime Institute of Biotechnology) and centrifuged at 12,000 x g for 30 min to collect the supernatant. The protein concentration was analyzed using a bicinchoninic acid kit (cat. no. P0010; Beyotime Institute of Biotechnology). Afterwards, the protein (20 μg/lane) was subjected to 10% sodium dodecyl sulfate-polyacrylamide gel electrophoresis and transferred onto a polyvinylidene fluoride membrane (39). The membrane was blocked with 5% skim milk at room temperature for 1 h. After it was washed with Tris-buffered saline with Tween (TBST) solution (20 mmol/l Tris-HCl, 5% non-fat milk, 150 mmol/l NaCl, and 0.05% Tween-20, pH 7.5) (5 min, 3 times), the membranes were incubated with rabbit anti-RBM15 (1:1,000; cat. no. ab315456; Abcam), rabbit anti-USF2 (1:2,000; cat. no. ab264330; Abcam), rabbit anti-IGF2BP3 (1:500; RRID: AB_2808308; cat. no. PA5-96506; Thermo Fisher Scientific, Inc.), rabbit anti-NLRP3 (1:500; cat. no. MA5-32255; Thermo Fisher Scientific, Inc.), rabbit anti-GSDMD-N (1:2,000; RRID: AB_3663000; cat. no. YT7991; ImmunoWay Biotechnology Company), rabbit anti-cleaved caspase-1 (1:500; RRID: AB_2818323; cat. no. PA5-99390; Thermo Fisher Scientific, Inc.), rabbit anti-caspase-1 (1:1,000; RRID: AB_2888675; cat. no. ab138483; Abcam) and rabbit anti-β-actin (1:1,000; RRID: AB_2305186; cat. no. ab8227; Abcam) at 4˚C overnight. After they were washed with TBST (5 min, 3 times), the membranes were incubated with the corresponding goat anti-rabbit secondary antibody (1:2,000; RRID: AB_2819160; cat. no. ab205718; Abcam) at room temperature for 1 h. The membranes were then washed with TBST (5 min, 3 times). Finally, the signal was detected by enhanced chemiluminescence (cat. no. 32132; Thermo Fisher Scientific Inc.), with β-actin used as a control. The film was exposed in a dark room, fixed, scanned with an Epson scanner (EPSON, V19ii/V39ii), and finally analyzed using Image-Pro Plus v6.0 (Media Cybernetics, Inc.).

RNA immunoprecipitation (RIP). The cells were lysed in RIPA lysis buffer (cat. no. 20-188; Sigma-Aldrich; Merck KGaA) containing an RNase inhibitor and a protein inhibitor for 30 min in an ice bath and then centrifuged at 16,000 x g for 10 min at 4˚C to obtain the supernatant. The preequilibrated protein A/G Sepharose beads were mixed with an appropriate amount of mouse anti-m6A (1:100; RRID: AB_3674612; cat. no. MABE1006; Sigma-Aldrich; Merck KGaA), rabbit anti-IGF2BP3 (1:100; cat. no. PA5-96506; Thermo Fisher Scientific, Inc.) or rabbit anti-USF2 (1:100; cat. no. ab264330; Abcam) and rotated at 4˚C for ~6 h. The supernatant was added to the bead-antibody mixture and rotated overnight at 4˚C, with IgG (1:100; RRID: AB_2687931; cat. no. ab172730; Abcam) used as the control. The mixed solution was centrifuged at 4˚C and 100 x g for 10 sec to remove the supernatant, after which it was washed twice with cold low-salt rinse solution in an ice bath (5 min each time) and then washed twice with high-salt rinse solution (5 min each time). RNA was extracted and subjected to RT-qPCR. The lysate was incubated overnight at 4˚C with a specific anti-Ago2 antibody (1:100; RRID: AB_2687492; cat. no. ab156870; Abcam) or control IgG (1:100; cat. no. ab172730; Abcam). After it was washed, the immunoprecipitated RNA was isolated by treatment with proteinase K and extraction with phenol/chloroform. The purified RNA was reverse transcribed, and the target RNAs (miR-195-5p and RBM15) were evaluated by RT-qPCR analysis (39).

m6A quantitative analysis. Total RNA was extracted using TRIzol reagent, and the m6A RNA level of total RNA was measured using a m6A RNA methylation quantification kit (cat. no. ab185912; Abcam) (51). The detection well was coated with RNA, followed by the addition of a capture antibody, detection antibody, and enhancer solution separately. Finally, the colorimetric solution was added, and the absorbance was measured at 450 nm. The m6A level was quantitatively analyzed by measuring the absorbance of each well.

Actinomycin D treatment. Actinomycin D (5 μg/ml; cat. no. A4262; Sigma-Aldrich; Merck KGaA) was added to the culture medium to block cell transcription (52), and the USF2 mRNA level was analyzed by RT-qPCR.

Chromatin immunoprecipitation (ChIP). At room temperature, the cells were crosslinked with 1% formaldehyde (cat. no. 47608; Sigma-Aldrich; Merck KGaA) for 10 min. After they were washed 4 times with 20 ml of PBS in a 50 ml conical tube, the cells were scraped and incubated on ice for 10 min. After they were centrifuged at 2,000 x g for 5 min, the cells were ultrasonicated by a Branson 150 Ultrasonic Processor. For ChIP, anti-USF2 antibody (1:100; cat. no. ab264330; Abcam) and anti-IgG antibody (1:100; cat. no. ab172730; Abcam) were used as negative controls. Specific primers (Table I) were used for PCR amplification of the USF2 binding region of the NLRP3 promoter (29).

Dual-luciferase assay. To investigate the interaction between miR-195-5p and RBM15, wild-type (WT) and mutant (MUT) RBM15 3'-untranslated regions (UTRs) containing putative binding sites for miR-195-5p were constructed. miR-195-5p mimics or NC mimics and reporter vectors (pmirGLO vector; Promega Corporation) containing WT or MUT RBM15 3'-UTRs were co-transfected into cells using Lipofectamine 3000. Similarly, to investigate the regulation of the *NLRP3* promoter by USF2, WT and MUT NLRP3 promoter sequences containing the putative binding site of *USF2* were constructed based on the psiCHECK-2 vector (Promega Corporation) and co-transfected with oe-USF2 or oe-NC using Lipofectamine 3000. Similarly, to investigate the regulation of the *USF2* m6A site by *RBM15* and *IGF2BP3*, WT and MUT sequences containing predicted USF2 m6A sites were constructed based on the psiCHECK-2 vector and co-transfected with oe-RBM15, oe-IGF2BP3, or oe-NC using Lipofectamine 3000. After 24 h of cultivation, the luciferase activity was measured using the luciferase assay system (Ambion; Thermo Fisher Scientific, Inc.). The ratio of the luminescence of firefly luciferase to that of *Renilla* luciferase was calculated (46).

Statistical analysis. Data analysis and map plotting were performed using SPSS 21.0 (IBM Corp.) and GraphPad Prism 8.0 (GraphPad Software Inc.; Dotmatics). All the data were tested for normality using the Shapiro-Wilk test. If the data between multiple groups did not follow a normal

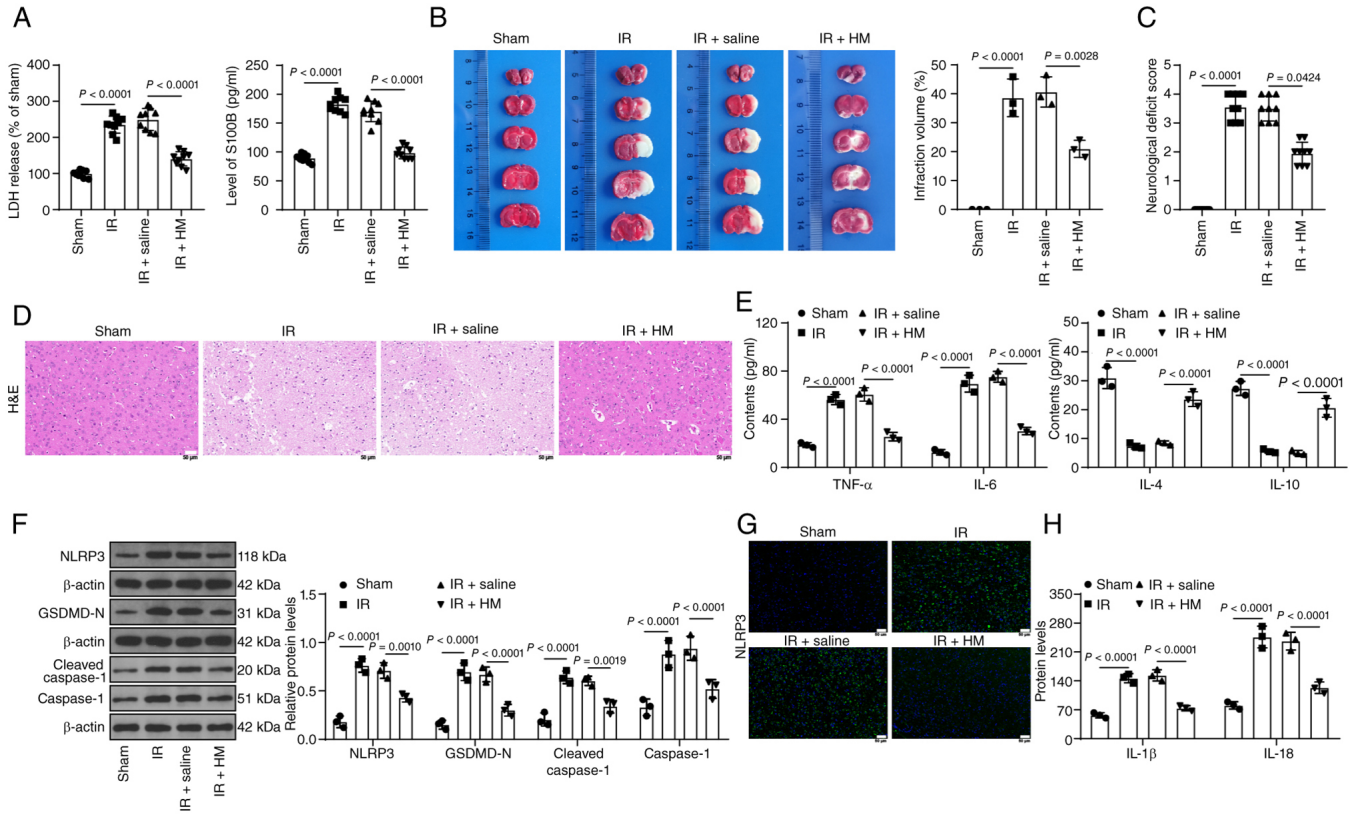

Figure 2. HM preconditioning alleviates cerebral I/R inflammatory injury in mice and represses NLRP3-mediated pyroptosis. The mice were treated according to the process shown in Fig. 1A. (A) LDH and S100B levels in the serum of each group of mice. (B) 2,3,5-triphenyltetrazolium chloride staining for detecting infarct size in brain tissue. (C) Neurological function scores of the mice in each group. (D) H&E staining for detecting brain tissue injury; magnification, x200. (E) ELISA detection of inflammatory factors in brain tissues. (F) Western blot analysis of the protein expression levels of NLRP3, GSDMD-N, caspase-1 and cleaved caspase-1 in brain tissues. (G) Immunofluorescence staining for detecting the percentage of NLRP3-positive brain tissues; magnification, x200. (H) ELISA detection of pyroptosis factors in brain tissues. Animal experiments in A and C: n=9; others: n=3. The data are expressed as the mean ± standard deviation. Comparisons between multiple groups in panel C were conducted using the Kruskal-Wallis test, and Dunn's multiple comparisons test was used for post hoc testing. The data in panels A and B were analyzed via one-way ANOVA, and the data in panels E, F and H were analyzed via two-way ANOVA, followed by Tukey's multiple comparisons test. HM, hydromorphone; I/R, ischemia/reperfusion; NLRP3, Nod-like receptor protein 3; LDH, lactate dehydrogenase; GSDMD, gasdermin D; IL, interleukin; TNF-α, tumor necrosis factor alpha.

distribution, a non-parametric test (Kruskal-Wallis test) was performed, followed by Dunn's multiple comparisons test. If the data between multiple groups followed a normal distribution, the Brown-Forsythe test was used for the homogeneity of variance test. To ensure homogeneity of variance, one-way analysis of variance (ANOVA) or two-way ANOVA was performed, with Tukey's multiple comparisons test or Sidak's multiple comparisons test for post hoc testing. If the data did not follow a normal distribution, a non-parametric test (Mann-Whitney test) was performed. If the data between two groups followed a normal distribution, a t-test was performed. The homogeneity of variance was determined using an F test. If equal variances were not assumed, the Welch t-test was performed again. P<0.05 was considered to indicate a statistically significant difference.

Results

HM preconditioning alleviates cerebral I/R inflammatory injury in mice and represses NLRP3-mediated pyroptosis. HM can protect against CIRI (12), but its mechanism is unclear. Middle cerebral artery occlusion/reperfusion (MCAO/R) mice were established and treated with HM (Fig. 1A). Compared with those in the sham group, the serum LDH and S100B levels in the IR group increased, whereas compared with those in the I/R + saline group, the serum LDH and S100B levels in the I/R + HM group decreased (P<0.01; Fig. 2A). After MCAO/R, the infarct volume of the mice increased, but HM preconditioning significantly reduced the infarct volume of the ischemic mice (P<0.01; Fig. 2B). As shown in Fig. 2C, HM preconditioning exerted neuroprotective effects (P<0.01). H&E staining revealed no significant abnormalities in the brain tissues of the sham-operated mice, whereas infarction accompanied by inflammatory cell infiltration was detected in the brain tissues of the MCAO/R-treated mice, but HM preconditioning improved these symptoms (Fig. 2D). After MCAO/R, the concentrations of the inflammatory factors TNF-α and IL-6 in brain tissues increased, whereas the concentrations of IL-4 and IL-10 decreased. However, HM preconditioning reversed these trends (P<0.01; Fig. 2E). HM inhibited pyroptosis (13), and the present results demonstrated that HM preconditioning significantly decreased the expression levels of NLRP3, GSDMD-N, caspase-1 and cleaved caspase-1 in brain tissues (P<0.01; Fig. 2F and G). Moreover, HM preconditioning also led to significant decreases in the concentrations of the pyroptosis factors IL-1β and IL-18

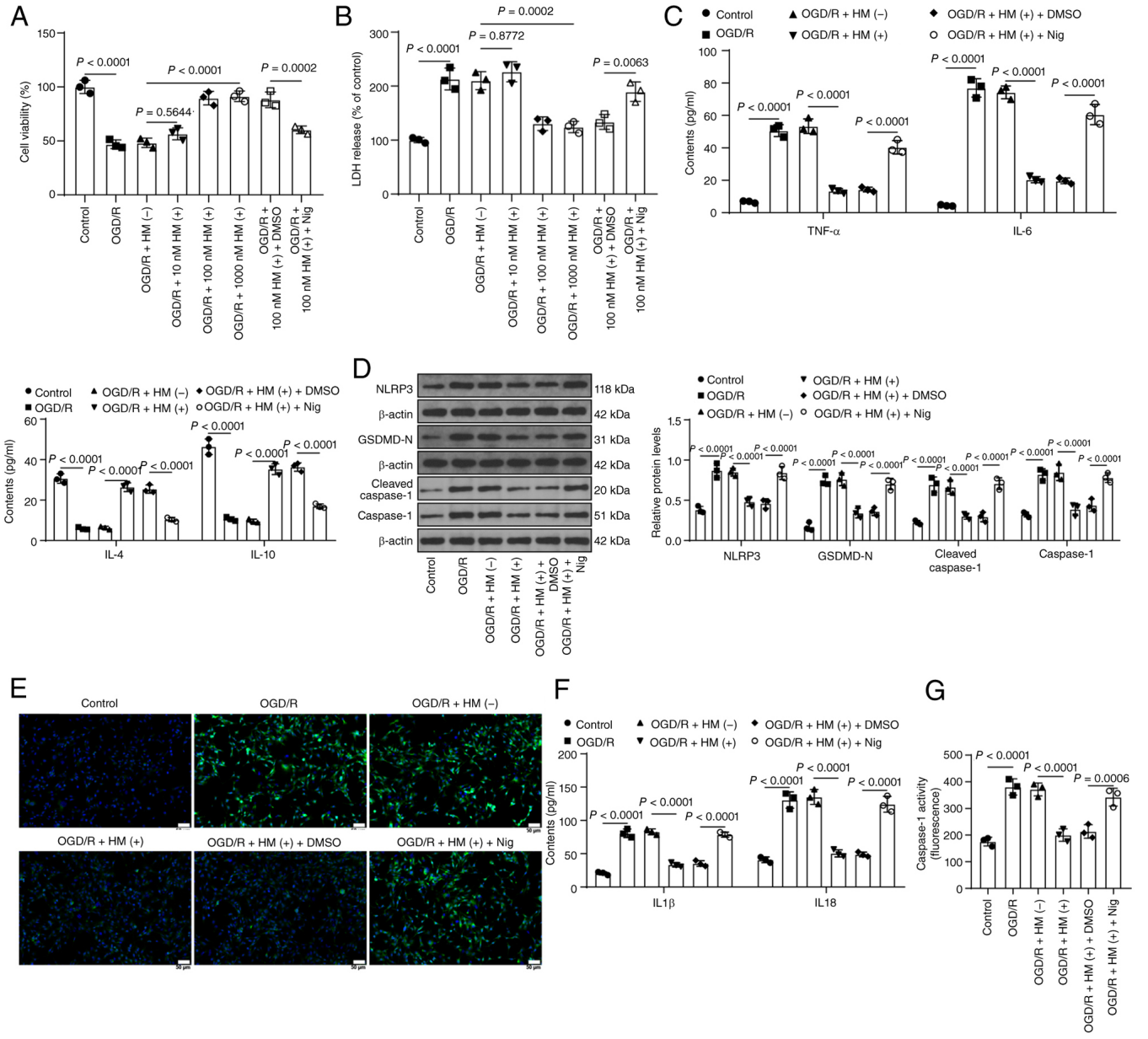

Figure 3. HM preconditioning alleviates OGD/R-induced inflammatory injury by repressing NLRP3-mediated pyroptosis. Cells were treated according to the process shown in Fig. 1B. (A) Cell Counting Kit-8 assay detection of cell viability. (B) LDH levels in each group of cells. (C) ELISA detection of inflammatory factors in cells. (D) Western blot analysis of the protein expression levels of NLRP3, GSDMD-N, caspase-1 and cleaved caspase-1 in cells. (E) Immunofluorescence staining for detecting the percentage of NLRP3-positive cells; magnification, x200. (F) ELISA detection of pyroptosis factors in cells. (G) Detection of caspase 1 enzyme activity using a caspase 1 fluorescence assay kit. A total of three technical replicates of the cell experiments were performed. The data are expressed as the mean ± standard deviation. The data in panels A, B and G were analyzed by one-way ANOVA, and the data in panels C, D and F were analyzed by two-way ANOVA, followed by Tukey's multiple comparisons test. HM, hydromorphone; OGD/R, oxygen-glucose deprivation/reperfusion; NLRP3, Nod-like receptor protein 3; GSDMD, gasdermin D; Nig, nigericin; IL, interleukin; TNF-α, tumor necrosis factor alpha.

(P<0.01; Fig. 2H). These results indicate that HM preconditioning alleviates cerebral I/R injury in mice and represses NLRP3-mediated pyroptosis.

HM preconditioning alleviates OGD/R-induced inflammatory injury by repressing NLRP3-mediated pyroptosis. Next, HBMVECs were induced with OGD/R (Fig. 1B) and a significant reduction in cell viability and an increase in LDH levels were observed, whereas HM preconditioning alleviated cell injury (P<0.01; Fig. 3A and B). HBMVECs were subsequently treated with 100 nM HM for further experiments. HM preconditioning reduced TNF-α and IL-6 levels induced by OGD/R but increased IL-4 and IL-10 levels inhibited by OGD/R (P<0.01; Fig. 3C). OGD/R upregulated the expression levels of NLRP3, GSDMD-N, caspase-1 and cleaved caspase-1, as well as the concentrations of IL-1β and IL-18 and the activity of caspase-1, but HM preconditioning decreased the expression levels of these factors (P<0.01; Fig. 3D-G). Furthermore, the NLRP3 agonist Nig was used in combination with HM. Compared with HM preconditioning alone, the combined treatment significantly increased pyroptosis but decreased cell viability, elevated LDH levels, and increased cell inflammation (P<0.01; Fig. 3A-G). Briefly, HM preconditioning alleviates OGD/R-induced inflammatory injury by repressing NLRP3-mediated pyroptosis.

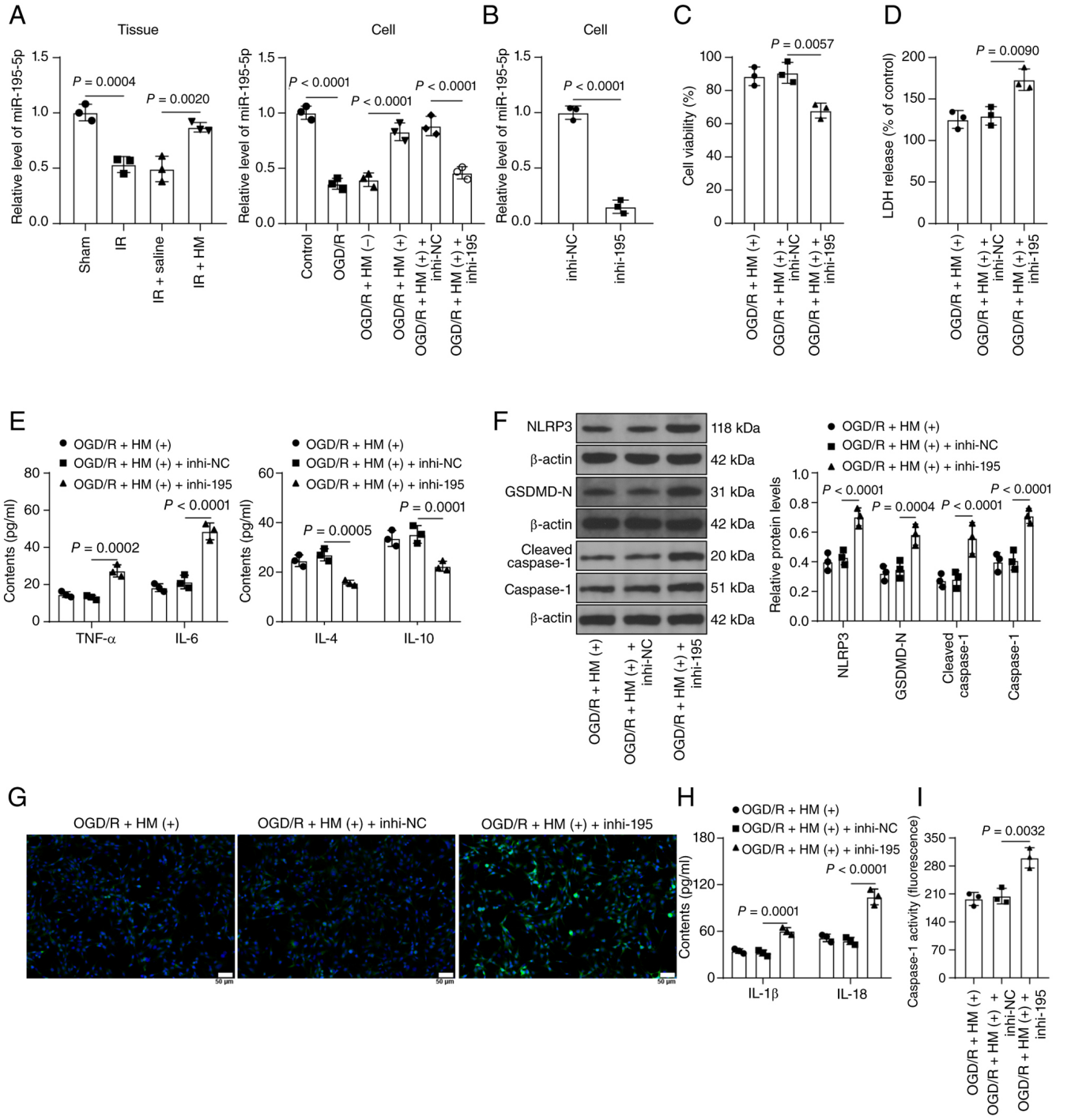

Figure 4. HM preconditioning alleviates OGD/R-induced inflammatory injury by upregulating the expression of miR-195-5p to suppress NLRP3-mediated pyroptosis. (A) RT-qPCR detection of the expression of miR-195-5p in brain tissues and cells; a miR-195-5p inhibitor (inhi-195) was transfected into human brain microvascular endothelial cells, with NC (inhi-NC) using as the negative control. (B) RT-qPCR detection of the transfection efficiency of miR-195-5p in cells. (C) Cell Counting Kit-8 assay detection of cell viability in each group. (D) LDH levels in each group of cells. (E) ELISA detection of inflammatory factors in cells. (F) Western blot analysis of the protein expression levels of NLRP3, GSDMD-N, caspase-1 and cleaved caspase-1 in cells. (G) Immunofluorescence staining for detecting the percentage of NLRP3-positive cells; magnification, x200. (H) ELISA detection of pyroptosis factors in cells. (I) Detection of caspase 1 enzyme activity using a caspase 1 fluorescence assay kit. Animal experiments: n=3. Three technical replicates of the cell experiments were performed. The data are expressed as the mean ± standard deviation. The data in panel B were analyzed via a t-test. The data in panels A, C, D and I were analyzed via one-way ANOVA, and the data in panels E, F and H were analyzed via two-way ANOVA, followed by Tukey's multiple comparisons test. HM, hydromorphone; OGD/R, oxygen-glucose deprivation/reperfusion; miR, microRNA; NLRP3, Nod-like receptor protein 3; RT-qPCR, reverse transcription-quantitative PCR; NC, negative control; LDH, lactate dehydrogenase; GSDMD, gasdermin D; I/R, ischemia/reperfusion; IL, interleukin; TNF-α, tumor necrosis factor alpha.

HM preconditioning alleviates OGD/R-induced inflammatory injury by upregulating the expression of miR-195-5p to suppress NLRP3-mediated pyroptosis. HM can regulate miRNA expression (53). miR-195-5p expression is reduced during CIRI (16,18), and miR-195-5p is associated with pyroptosis (19). It was hypothesized that miR-195-5p may be a downstream miRNA target of HM. The expression of miR-195-5p decreased in the model group but increased in the

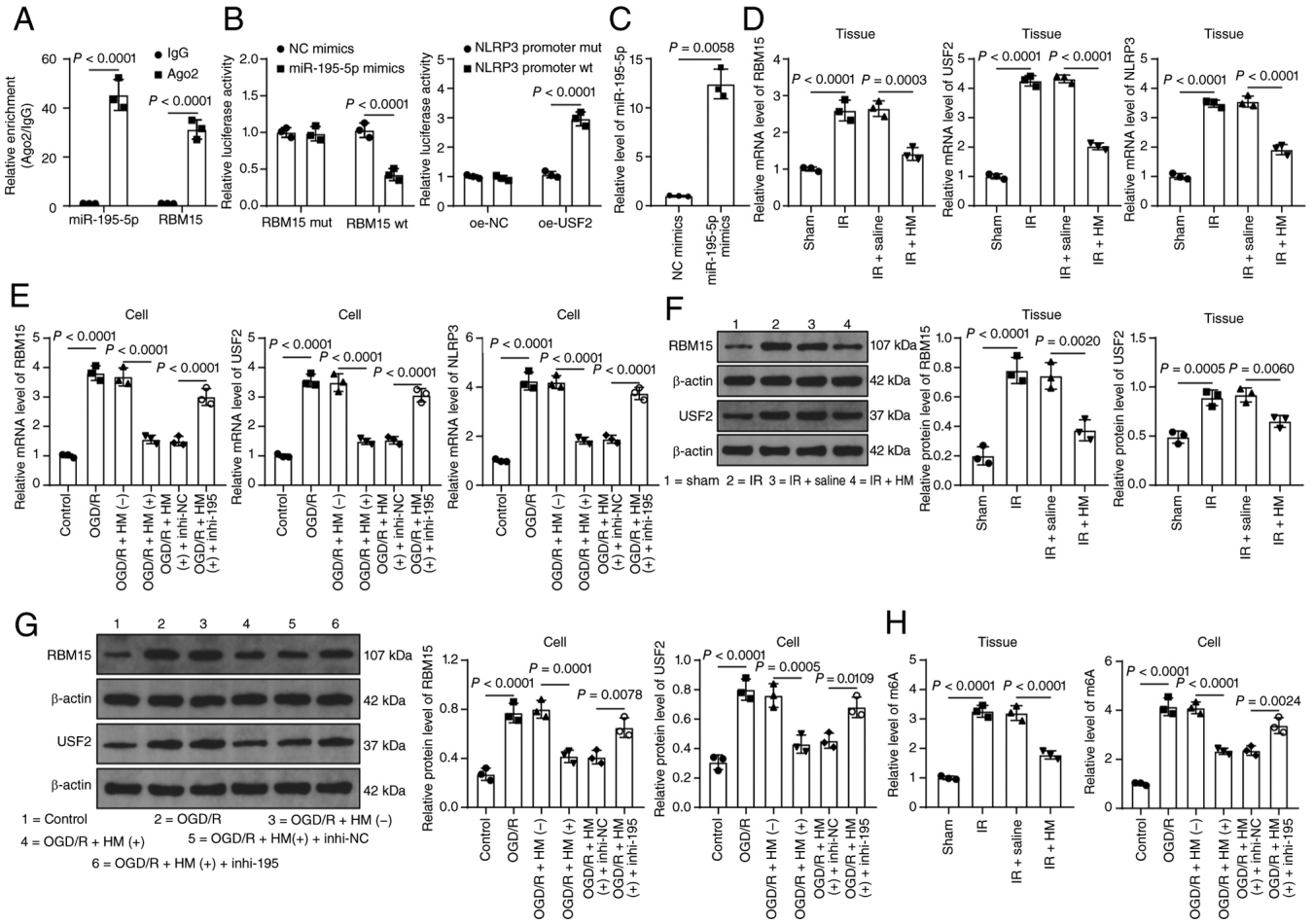

Figure 5. miR-195-5p targets RBM15 and reduces USF2 expression. (A) RNA immunoprecipitation detection of the binding relationship between miR-195-5p and RBM15. (B) Verification of the binding relationship by dual-luciferase assay. (C) RT-qPCR detection of miR-195-5p expression. (D and E) RT-qPCR detection of the mRNA expression levels of RBM15, USF2 and NLRP3 in brain tissues and cells. (F and G) Western blot detection of the protein expression levels of RBM15 and USF2 in brain tissues and cells. (H) Quantitative analysis of m6A content in brain tissues and cells. Animal experiments: n=3. A total of three technical replicates of the cell experiments were performed. The data are expressed as the mean ± standard deviation. The data comparisons between two groups in panel C were conducted using the Welch t-test. Comparisons between multiple groups in panels A and B were conducted using two-way ANOVA, and Sidak's multiple comparisons test was used for post hoc testing. The data in panels D-H were analyzed via one-way ANOVA, followed by Tukey's multiple comparisons test. miR, microRNA; RBM15, RNA-binding motif protein 15; USF2, upstream stimulatory factor 2; RT-qPCR, reverse transcription-quantitative PCR; NLRP3, Nod-like receptor protein 3; m6A, N6-methyladenosine; HM, hydromorphone; OGD/R, oxygen-glucose deprivation/reperfusion; I/R, ischemia/reperfusion; NC, negative control; oe-, overexpression; WT, wild-type; MUT, mutant.

HM preconditioning group (P<0.01; Fig. 4A). Considering that the pretreatment effect of HM has been verified in Fig. 3 (the negative control of HM is demonstrated in Fig. 3), the combined experiment was set up on the basis of Fig. 3. miR-195-5p expression was inhibited in HBMVECs, followed by OGD/R treatment in combination with HM (P<0.01; Fig. 4A and B). After inhibition of miR-195-5p expression, cell viability decreased, and LDH levels increased (P<0.01; Fig. 4C and D). Moreover, inhibition of miR-195-5p led to increases in the concentrations of TNF-α and IL-6 in cells, decreases in the concentrations of IL-4 and IL-10 (P<0.01; Fig. 4E), and significant increases in pyroptosis (P<0.01; Fig. 4F-I). These results suggest that HM preconditioning alleviates OGD/R-induced inflammatory injury by upregulating the expression of miR-195-5p to repress NLRP3-mediated pyroptosis.

miR-195-5p targets RBM15 and reduces USF2 expression, thus transcriptionally inhibiting NLRP3 expression. The downstream target genes of miR-195-5p were predicted (Fig. 1C) and it was reported that RBM15 was upregulated in cerebral I/R (21), but its role remains unclear. Therefore, RBM15 was chosen as the downstream target gene of miR-195-5p. RIP and dual-luciferase assays confirmed the target binding of miR-195-5p and the RBM15 3'-UTR (P<0.01; Fig. 5A-C). RBM15 expression increased in the model group but decreased in the HM preconditioning group (P<0.01; Fig. 5D-G), and after inhibition of miR-195-5p, RBM15 expression increased again (P<0.01; Fig. 5E and G). RBM15 functions as a m6A methyltransferase, and USF2 has m6A modification levels (Fig. 1D). USF2 expression is increased in cerebral I/R (29). Therefore, USF2 was chosen as a downstream factor of RBM15. It was found that the change in m6A content was consistent with the trend in RBM15 expression (P<0.01; Fig. 5H) and was accompanied by the enrichment of m6A in USF2 (P<0.01; Fig. 6A). Furthermore, a dual-luciferase assay was performed to determine the binding of RBM15 to USF2 m6A. The results revealed that the luciferase activity of the oe-RBM15 group was significantly greater than that of the oe-NC group (P<0.01;

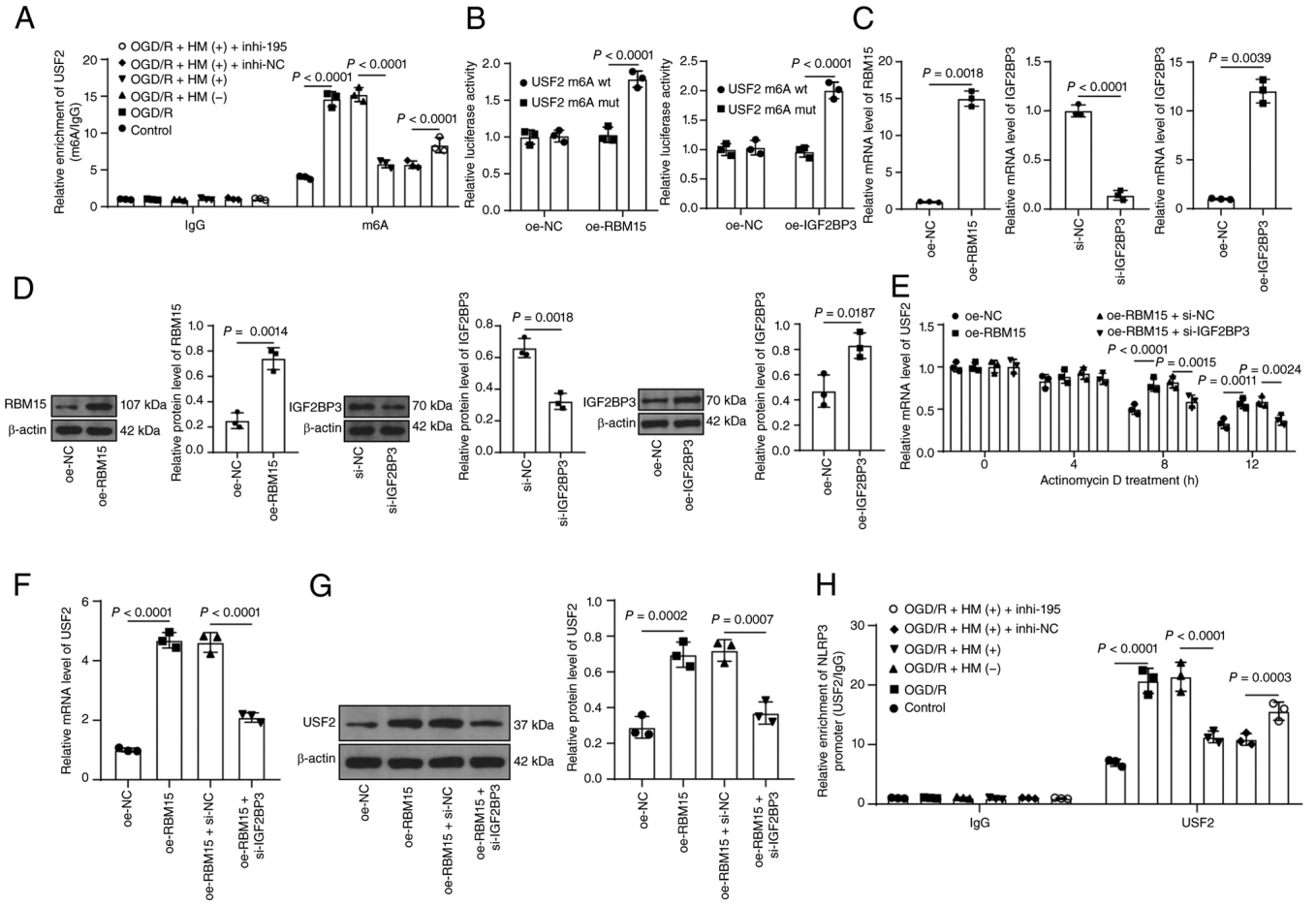

Figure 6. miR-195-5p inhibits NLRP3 expression via the RBM15/USF2 axis. (A) RNA immunoprecipitation analysis of USF2 m6A modification in each group of cells. (B) Dual-luciferase assay for detecting the binding of RBM15 and IGF2BP3 to USF2 m6A. (C and D) RT-qPCR and western blot analysis of the transfection efficiency of RBM15 and IGF2BP3 in cells. (E) RT-qPCR detection of the mRNA stability of USF2 in cells. (F and G) The expression of USF2 in cells was detected by RT-qPCR and western blotting. (H) Chromatin immunoprecipitation analysis of the enrichment of USF2 on the NLRP3 promoter in each group of cells. Animal experiments: n=3. Three technical replicates of the cell experiments were performed. The data are expressed as the mean ± standard deviation. The data comparisons between two groups in panel C (left, right) were conducted using the Welch t-test, while the data comparisons between two groups in panels C (middle) and D were conducted using the t-test. Comparisons between multiple groups in panel B were conducted using two-way ANOVA, and Sidak's multiple comparisons test was used for post hoc testing. The data in panels F and G were analyzed via one-way ANOVA, and the data in panels A, E and H were analyzed via two-way ANOVA, followed by Tukey's multiple comparisons test. miR, microRNA; NLRP3, Nod-like receptor protein 3; RBM15, RNA-binding motif protein 15; USF2, upstream stimulatory factor 2; RT-qPCR, reverse transcription-quantitative PCR; IGF2BP3, insulin-like growth factor 2 mRNA-binding protein 3; m6A, N6-methyladenosine; HM, hydromorphone; OGD/R, oxygen-glucose deprivation/reperfusion; si-, small interfering; NC, negative control; oe-, overexpression.

Fig. 6B). Moreover, overexpression of RBM15 significantly increased the mRNA stability and expression of USF2 (P<0.01; Fig. 6C-G). As a m6A-reading protein, IGF2BP3 often participates in the regulation of m6A modification by RBM15 (52). Similarly, the luciferase activity of the oe-IGF2BP3 group was significantly greater than that of the oe-NC group (P<0.01; Fig. 6B-D). After silencing of IGF2BP3, the mRNA stability and expression of USF2 decreased (P<0.01; Fig. 6C-G). USF2 expression increased in the model group but decreased in the HM preconditioning group. However, after inhibition of miR-195-5p, USF2 expression increased again (P<0.01; Fig. 5D-G). USF2, a transcription factor, is predicted by the JASPAR database to bind to the NLRP3 promoter (Fig. 1E). The ChIP results revealed that the enrichment trend of USF2 in the NLRP3 promoter was consistent with the expression trends of USF2 and NLRP3 (P<0.01; Fig. 6H). Dual-luciferase assays confirmed the binding of USF2 to the NLRP3 promoter (P<0.01; Fig. 5B), and the expression trend of NLRP3 was consistent with that of USF2 (P<0.01; Fig. 5D and E). In short, miR-195-5p targets RBM15 and reduces USF2 expression through IGF2BP3-mediated m6A modification, ultimately leading to the transcriptional inhibition of NLRP3 expression.

Overexpression of RBM15/USF2 abolishes the protective effect of HM preconditioning on OGD/R-induced pyroptosis. To verify the role of RBM15 in the ability of HM to protect against OGD/R-induced cell injury, the combined experiment was set up on the basis of Fig. 3 as the pretreatment effect of HM has been verified in Fig. 3 (the negative control of HM is shown in Fig. 3). RBM15 expression was upregulated in cells for a combined treatment with HM (P<0.05; Fig. 7A and C). As a result, the m6A content increased, and the m6A enrichment of USF2 in cells increased (P<0.05; Fig. 7E and F). After overexpression of RBM15, USF2 expression increased, and enrichment of USF2 in the NLRP3 promoter increased (P<0.05; Fig. 7A, D and G). NLRP3 expression also increased

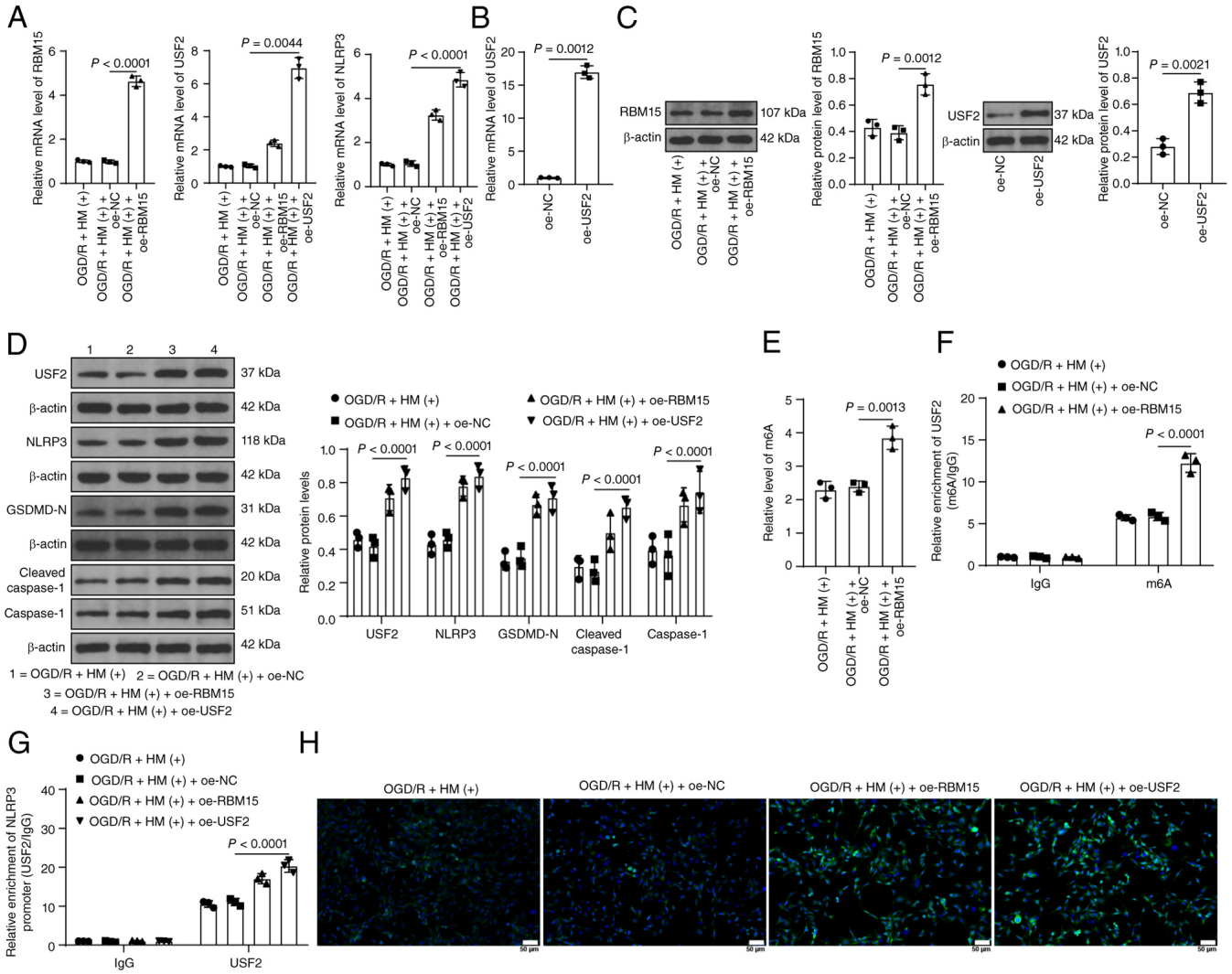

Figure 7. RBM15 promotes NLRP3 expression by upregulating USF2. The overexpression plasmids oe-RBM15 and oe-USF2 were transfected into human brain microvascular endothelial cells, with the empty vector pcDNA3.1 (oe-NC) as a negative control. (A) RT-qPCR detection of the mRNA expression levels of RBM15, USF2 and NLRP3 in cells. (B) RT-qPCR detection of the transfection efficiency of USF2 in cells. (C and D) Western blot detection of protein expression. (E) Quantitative analysis of m6A content in cells. (F) RNA immunoprecipitation analysis of USF2 m6A modification in each group of cells. (G) Chromatin immunoprecipitation analysis of the enrichment of USF2 on the NLRP3 promoter in each group of cells. (H) Immunofluorescence staining for detecting the percentage of NLRP3-positive cells; magnification, x200. A total of three technical replicates of the cell experiments were performed. The data are expressed as the mean ± standard deviation. The data in panel B were analyzed via the Welch t-test, while the data comparisons between two groups in panel C (right) were conducted using the t-test. The data in panels A, C (left) and E were analyzed via one-way ANOVA, and the data in panels D, F and G were analyzed via two-way ANOVA, followed by Tukey's multiple comparisons test. RBM15, RNA-binding motif protein 15; NLRP3, Nod-like receptor protein 3; USF2, upstream stimulatory factor 2; oe-, overexpression; NC, negative control; RT-qPCR, reverse transcription-quantitative PCR; m6A, N6-methyladenosine; HM, hydromorphone; OGD/R, oxygen-glucose deprivation/reperfusion; GSDMD, gasdermin D.

accordingly (P<0.05; Fig. 7A, D and H). In addition, overexpression of RBM15 led to a decrease in cell viability, an increase in LDH levels, and a significant increase in inflammatory and pyroptosis levels (P<0.05; Figs. 7D and H; 8A-E), alleviating the protective effect of HM preconditioning on OGD/R-induced pyroptosis.

To verify the role of USF2 in the protective effect of HM against OGD/R-induced cell injury, the combined experiment was set up on the basis of Fig. 3 as the pretreatment effect of HM has been verified in Fig. 3 (the negative control of HM is shown in Fig. 3). USF2 expression was upregulated in cells for a combined treatment with HM (P<0.05; Fig. 7A-D), which resulted in an increase in USF2 enrichment in the NLRP3 promoter (P<0.05; Fig. 7G) and an increase in NLRP3 expression (P<0.05; Fig. 7A, D and H). Overexpression of USF2 also counteracted the protective effect of HM preconditioning on OGD/R-induced cell pyroptosis (P<0.05; Figs. 7D and H; 8A-E).

HM preconditioning alleviates cerebral I/R injury in mice by upregulating the expression of miR-195-5p to repress NLRP3-mediated pyroptosis. Finally, to validate *in vitro* results, the combined experiment was set up on the basis described in Fig. 2, as the pretreatment effect of HM has been verified in (the negative control of HM is shown in Fig. 2). miR-195-5p expression was reduced in the mouse brain (P<0.01; Fig. 9A and B), which resulted in increases in m6A content and RBM15, USF2 and NLRP3 expression levels (P<0.01; Fig. 9B-D). After inhibition of miR-195-5p expression, the serum LDH and S100B levels in mice increased, and the infarct volume increased, indicating a decrease in the neuroprotective effect of HM preconditioning

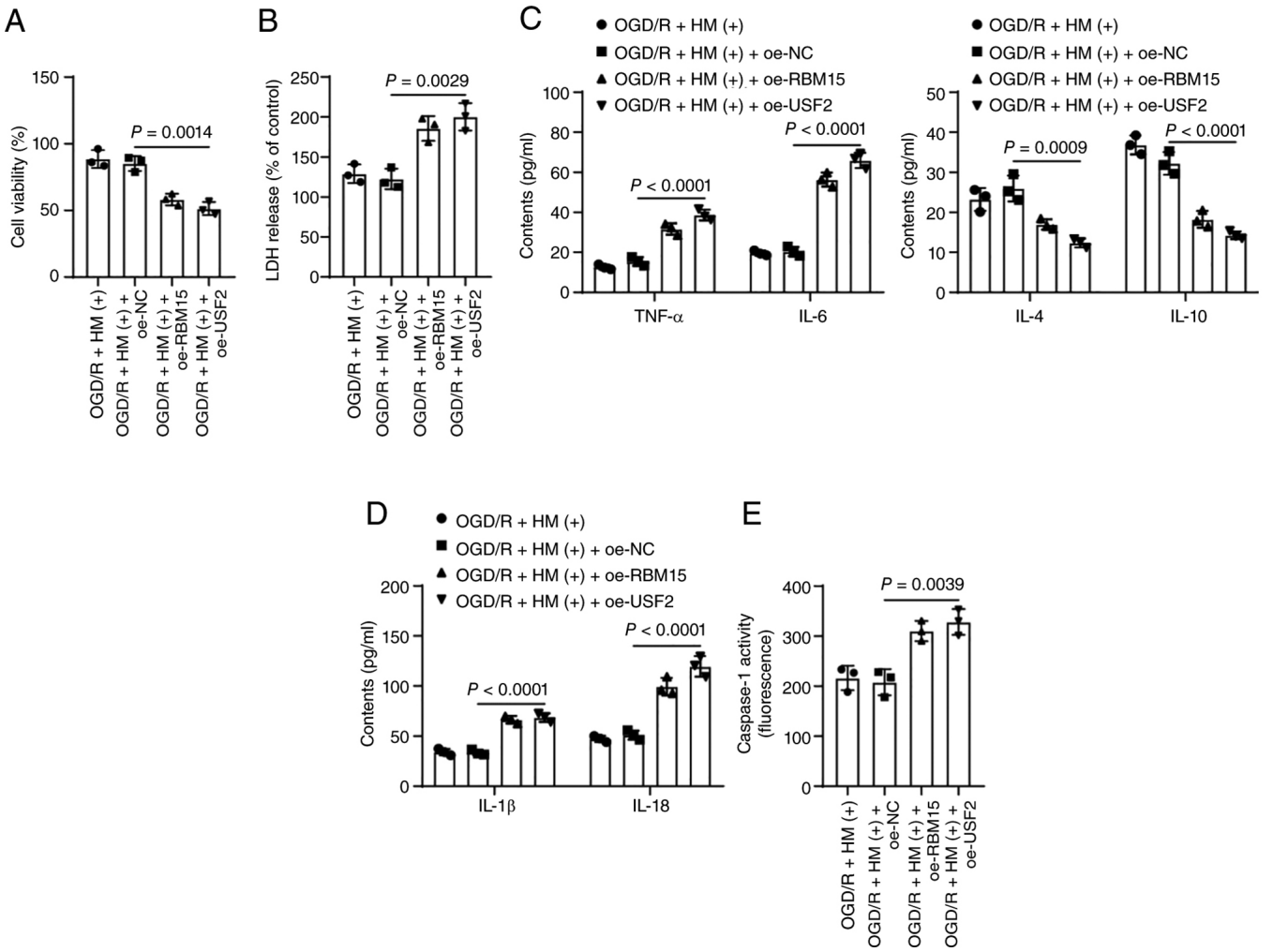

Figure 8. Overexpression of RBM15/USF2 abolishes the protective effect of HM preconditioning on OGD/R-induced pyroptosis. (A) Cell Counting Kit-8 assay detection of cell viability in each group. (B) LDH levels in each group of cells. (C and D) ELISA detection of inflammatory factors and pyroptosis factors in cells. (E) Detection of caspase 1 enzyme activity using a caspase 1 fluorescence assay kit. A total of three technical replicates of the cell experiments were performed. The data are expressed as the mean ± standard deviation. The data in panels A, B and E were analyzed via one-way ANOVA, and the data in panels C and D were analyzed via two-way ANOVA, followed by Tukey's multiple comparisons test. RBM15, RNA-binding motif protein 15; USF2, upstream stimulatory factor 2; OGD/R, oxygen-glucose deprivation/reperfusion; LDH, lactate dehydrogenase; HM, hydromorphone; oe-, overexpression; NC, negative control; IL, interleukin; TNF-α, tumor necrosis factor alpha.

(P<0.05; Fig. 9E-G). H&E staining revealed that the brain tissues of mice in which miR-195-5p was inhibited exhibited infarction accompanied by inflammatory cell infiltration (Fig. 9I). The inhibition of miR-195-5p exacerbated inflammatory injury in brain tissues (P<0.01; Fig. 9J) and increased the expression levels of NLRP3, GSDMD-N, caspase-1 and cleaved caspase-1 (P<0.01; Fig. 9C and I), as well as the concentrations of IL-1β and IL-18 (P<0.01; Fig. 9H). Briefly, inhibition of miR-195-5p promotes NLRP3-mediated pyroptosis by upregulating the RBM15/USF2 axis and alleviating the protective effect of HM preconditioning on inflammatory injury in mice with cerebral I/R.

Discussion

NLRP3 inflammasome-mediated pyroptosis is a vital pathological link in the inflammatory response to CIRI (1). HM is a potent opioid analgesic commonly administered in acute care settings (54). The present study revealed that HM preconditioning downregulates the RBM15/USF2 axis by upregulating the expression of miR-195-5p, thus repressing NLRP3-mediated pyroptosis and ultimately alleviating CIRI (Fig. 10).

HM is an opioid analgesic with a strong analgesic effect, long duration, and few adverse events (55). In terms of pharmacodynamics, the analgesic effect of HM is 5-10-fold greater than that of the equivalent dose of morphine (56). A double-blind, randomized and controlled trial revealed that preoperative 2 mg of HM in patients undergoing laparoscopic radical gastrectomy can reduce intraoperative changes in blood pressure and heart rate and relieve postoperative pain intensity (57). In the present study, it was revealed that HM preconditioning notably reduced the infarct size of MCAO/R mice, alleviated inflammatory cell infiltration in brain tissues, and diminished inflammatory cytokines in brain tissues. Additionally, HM has been demonstrated to protect hippocampal neurons from I/R injury by activating mTOR signaling (12). Pyroptosis is a type of proinflammatory cell death that occurs in an NLRP3-dependent manner

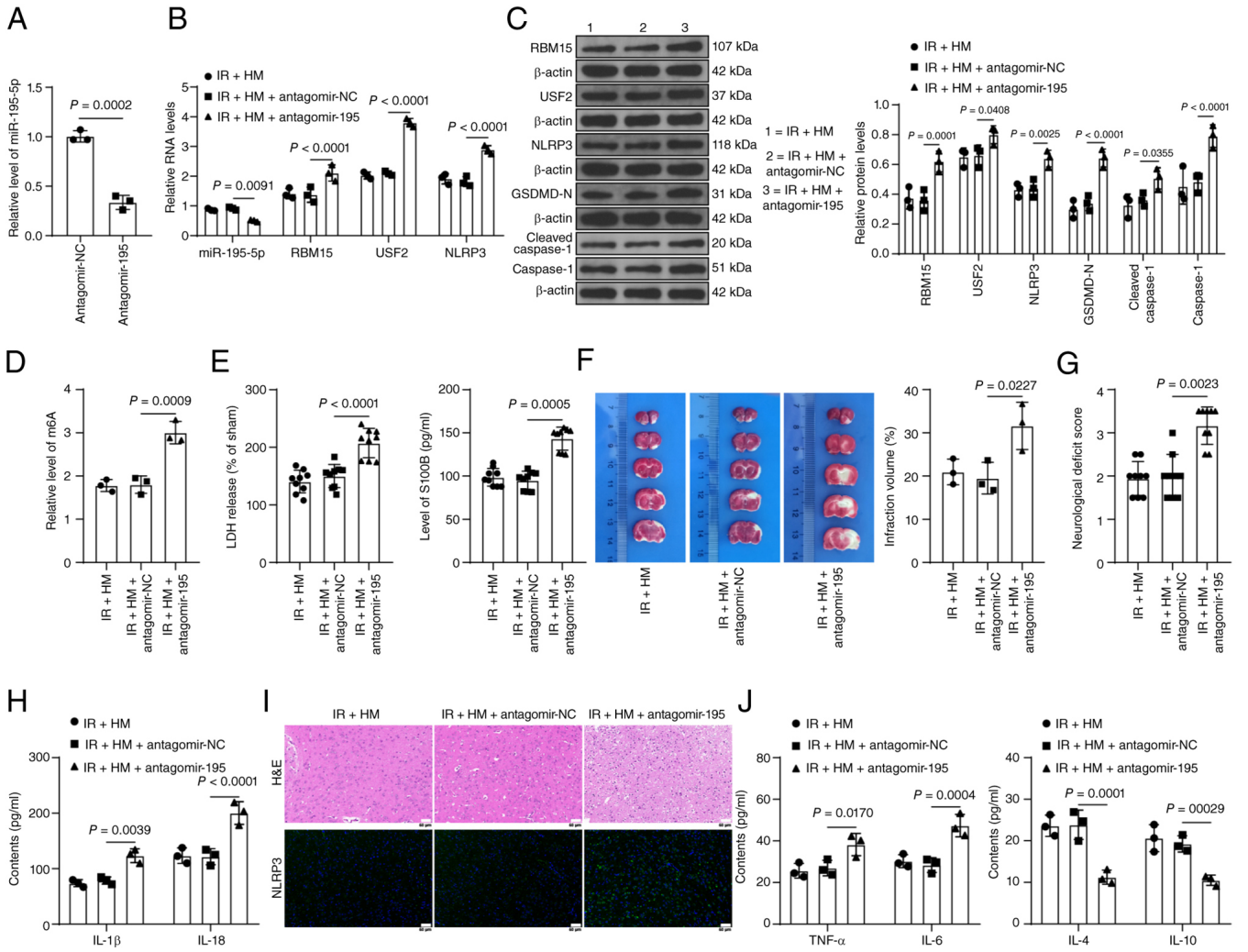

Figure 9. HM preconditioning alleviates mouse cerebral I/R injury by upregulating the expression of miR-195-5p to repress NLRP3-mediated pyroptosis. The mice were treated according to the process shown in Fig. 1A. (A) RT-qPCR detection of the miR-195-5p transfection efficiency in brain tissues. (B) RT-qPCR detection of the RNA expression of various genes in brain tissues. (C) Western blot detection of the protein expression levels of various proteins in brain tissues. (D) Quantitative analysis of m6A content in brain tissues. (E) LDH and S100B levels in the serum of mice. (F) 2,3,5-Triphenyltetrazolium chloride staining for detecting infarct size in brain tissues. (G) Neurological function scores of the mice in each group. (H) ELISA detection of pyroptosis factors in brain tissues. (I) Tissue staining for detecting brain tissue injury and the positive rate of NLRP3 expression. (J) ELISA detection of inflammatory factors in brain tissues. Animal experiments in panels E and G: n=9; others: n=3. The data are expressed as the mean ± standard deviation. Comparisons between two groups in panel A were conducted using the t-test; comparisons between multiple groups in panels E (right) and G were conducted using the Kruskal-Wallis test, and Dunn's multiple comparisons test was used for post hoc testing. The data in panels D, E (left) and F were analyzed via one-way ANOVA, and the data in panels B, C, H and J were analyzed via two-way ANOVA, followed by Tukey's multiple comparisons test. HM, hydromorphone; I/R, ischemia/reperfusion; miR, microRNA; NLRP3, Nod-like receptor protein 3; RT-qPCR, reverse transcription-quantitative PCR; m6A, N6-methyladenosine; LDH, lactate dehydrogenase; RBM15, RNA-binding motif protein 15; USF2, upstream stimulatory factor 2; NC, negative control; IL, interleukin; TNF-α, tumor necrosis factor alpha.

after CIRI (4,58). HM preconditioning significantly reduced the expression levels of NLRP3, GSDMD-N and cleaved caspase-1 in the brain tissues of MCAO/R mice, as well as the concentrations of the pyroptosis factors IL-1β and IL-18, indicating that HM preconditioning alleviated CIRI and restrained NLRP3-mediated pyroptosis in MCAO/R mice. Consistently, it has been reported that HM represses NLRP3 inflammasome-mediated pyroptosis in alveolar macrophages by upregulating Nrf2/HO-1 expression (13). *In vitro*, it was found that HM preconditioning reduced OGD/R-induced inflammatory factor expression and suppressed pyroptosis in HBMVECs. After combined treatment with the NLRP3 agonist Nig and HM, cell pyroptosis significantly increased, but cell viability decreased and the inflammatory response increased, indicating that HM preconditioning alleviated OGD/R-induced inflammatory injury by suppressing NLRP3-mediated pyroptosis.

Thereafter, it was attempted to determine the underlying mechanism through which HM preconditioning alleviates CIRI. miRNAs positively modulate inflammation and cell survival/death in response to CIRI (59). miRNA features can be utilized as clinical biomarkers for predicting the analgesic effect of HM (53). The overexpression of miR-195-5p efficiently increased cell viability while reducing LDH release and apoptosis in OGD-induced HBMVECs *in vitro* and ameliorating cerebral injury in MCAO mice *in vivo* (16). Silencing of miR-195-5p exacerbates inflammation and apoptosis in OGD/R-induced HT22 cells (18). miR-195-5p attenuates pyroptosis in OGD/R-induced GC-1 cells by repressing PELP1 expression (19). Similarly, it was found that miR-195-5p

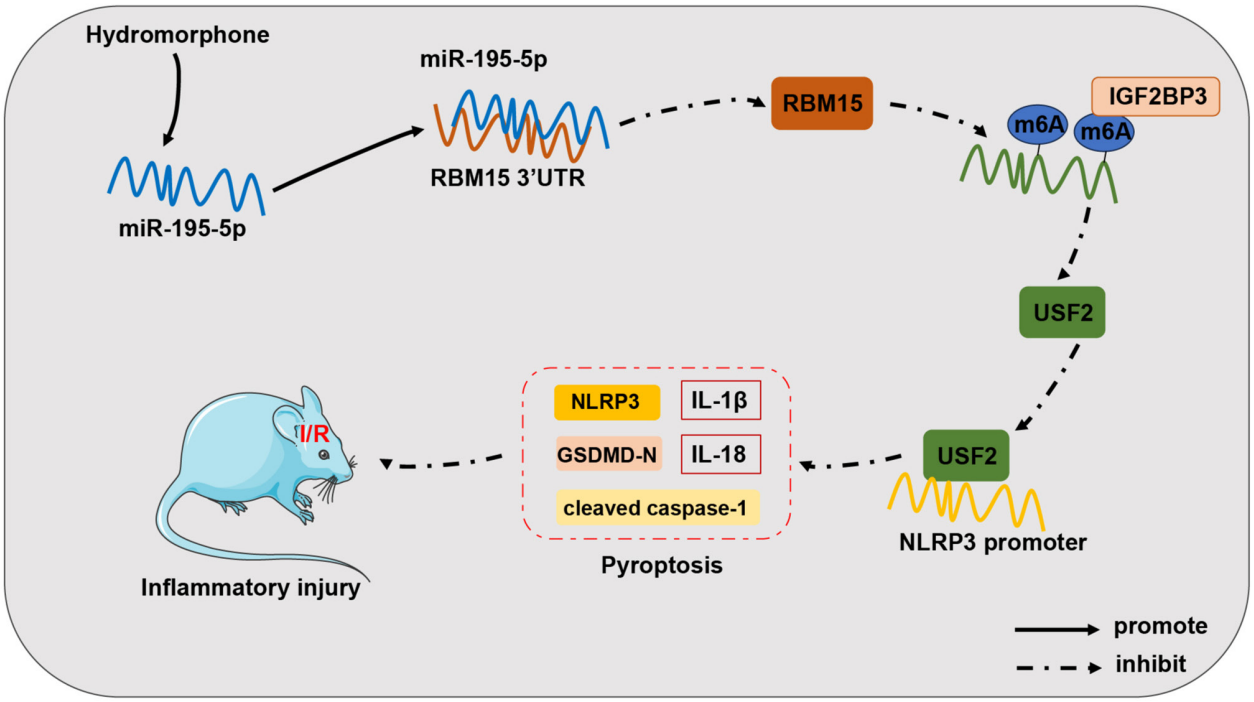

Figure 10. Mechanism through which HM preconditioning alleviates inflammatory injury caused by cerebral I/R injury. HM preconditioning can upregulate miR-195-5p expression, target RBM15 expression, reduce IGF2BP3-mediated m6A modification, and decrease USF2 expression, thus reducing the enrichment of USF2 on the NLRP3 promoter, inhibiting NLRP3-mediated pyroptosis, and alleviating cerebral I/R inflammatory injury. I/R, ischemia/reperfusion; HM, hydromorphone; miR, microRNA; RBM15, RNA-binding motif protein 15; m6A, N6-methyladenosine; USF2, upstream stimulatory factor 2; NLRP3, Nod-like receptor protein 3; UTR, untranslated region; IGF2BP3, insulin-like growth factor 2 mRNA-binding protein 3.

expression decreased in the model group but increased in the HM preconditioning group. The inhibition of miR-195-5p expression decreased cell viability, elevated cellular inflammation, and significantly enhanced pyroptosis. These results indicated that HM preconditioning alleviated OGD/R-induced inflammatory injury by upregulating the expression of miR-195-5p to inhibit NLRP3-mediated pyroptosis.

Furthermore, the target genes downstream of miR-195-5p were predicted. The binding between miR-195-5p and RBM15 was confirmed by a dual-luciferase assay. RBM15 expression is upregulated after cerebral ischemia (21). The silencing of RBM15 diminishes inflammatory factors and decreases pyroptosis in high glucose-induced HK-2 cells (24). The present results demonstrated that RBM15 expression increased in the model group but decreased in the HM preconditioning group, but RBM15 expression increased again after inhibition of miR-195-5p. USF2 belongs to the bHLH-LZ transcription factor family and interacts with the E-box of the DNA-core sequence in its target genes (60). USF2 is crucial for controlling growth and developmental processes, as it affects embryonic development, fertility and brain function (61). m6A modification was detected on USF2, and the changes in m6A content in USF2 were consistent with the expression trends of RBM15. Overexpression of RBM15 significantly promoted the mRNA stability and expression of USF2. USF2 is highly expressed in MCAO mice, and knockdown of USF2 markedly reduces autophagy and alleviates CIRI (29). USF2 increases NLRP3 expression at the transcriptional level, and inhibition of USF2 represses the pyroptosis of podocytes and relieves kidney injury in patients with lupus nephritis (62). It was also revealed that HM preconditioning limited the upregulation of USF2 expression in MCAO mice and OGD/R-induced HBMVECs. Functional rescue experiments confirmed that overexpression of RBM15/USF2 abolished the protective effect of HM preconditioning on OGD/R-induced pyroptosis. Finally, to validate the *in vitro* results, miR-195-5p expression was reduced in mice and it was found that inhibition of miR-195-5p exacerbated inflammatory injury to the brain tissue and increased pyroptosis, indicating that inhibition of miR-195-5p facilitated NLRP3-mediated pyroptosis by upregulating the RBM15/USF2 axis and reversing the protective effect of HM preconditioning on CIRI in mice.

In conclusion, HM preconditioning upregulates miR-195-5p expression to suppress RBM15 expression, reduces IGF2BP3-mediated m6A modification, and decreases USF2 expression, thus reducing USF2 enrichment on the NLRP3 promoter, repressing NLRP3-mediated pyroptosis, and alleviating CIRI. The present study provides new strategies and targets for the treatment of CIRI. Multicenter preclinical studies are needed to further clarify the neuroprotective effects of HM, which is expected to fill the gap in existing neuroprotective drugs.

However, the present study has certain limitations. First, long-term functional assessments are lacking. Owing to the limited funding and experimental technology in the authors' research group, the functional outcomes of the mice by adhesive removal, rotarod and corner tests were not assessed. In addition, additional experiments on the combination of MCC950 or Nlrp3$^{-/-}$ mice were not conducted. MCC950 or Nlrp3$^{-/-}$ mice will be used for deeper validation in future studies. Second, only endothelial cells were used *in vitro*. Considering that human-derived cells are more closely related

to the clinical pathological environment, HBMVECs were chosen as the objective cells but did not replicate key nodes of the mechanism in primary murine brain microvascular endothelial cells. Hence, cross-species limitations such as differences in inflammatory response and culture conditions may affect the results. In the combined experiments, the data of OGD/R^+ (HM^-) and IR^+ saline groups in Figs. 4, 6 and 7 were not shown, which were the negative controls of HM in the *in vitro* and *in vivo* experiments. Third, the absence of antagonist experiments (for example, naloxone) render unclear whether the protective effects of HM are mediated by opioid receptors. Fourth, although a combined experiment involving HM preconditioning and genetic intervention was conducted, the causal relationship using caspase-1 inhibitors to enhance the rigor of the manuscript has not yet been validated. Fifth, a seed-mutant RBM15 3'UTR (insensitive to miR-195-5p) in AGO2-RIP assay was not used. This experiment may be included in future studies to further confirm the target binding of miR-195-5p to RBM15. Moreover, ChIP and RIP assays merely included IgG as a negative control, but did not include positive control loci. Last but not least, only miR-195-5p was selected as the downstream target of HM, and whether other potential off-target miRNAs are involved remains unclear. For the downstream target of miR-195-5p, only RBM15 was selected as the target gene from the database. It is unknown whether RBM15 affects USF2 through other m6A readers, and additional genes downstream of RBM15 remain to be clarified.

As the present study remains in the exploratory stage, more experimental evidence is needed to apply the conclusions to clinical testing. In the future, other downstream mechanisms of HM preconditioning will be explored through differential analysis to further elucidate the impact of HM preconditioning on CIRI and provide new theoretical knowledge for the treatment of CIRI.

Acknowledgements

Not applicable.

Funding

No funding was received.

Availability of data and materials

The data generated in the present study may be requested from the corresponding author.

Authors' contributions

JY conceptualized the study, visualized, curated and validated data, conducted formal analysis, developed methodology, wrote the original draft, and wrote, reviewed and edited the manuscript. ZH conceptualized the study, curated and visualized data, and conducted investigation. SL supervised the study, curated and validated data, and developed methodology. ML conceptualized the study, conducted formal analysis and investigation, and developed methodology. JF supervised the study, conducted formal analysis and investigation, validated data, and wrote, reviewed and edited the manuscript. JY and YF confirm the authenticity of all the raw data. All authors read and approved the final version of the manuscript.

Ethics approval and consent to participate

The study procedure was approved by the Ethics Committee of Liaoning Cancer Hospital and Institute (approval no. CMU20250031; Shenyang, China). All animal experiment schemes were approved by the Animal Ethics Committee of Liaoning Cancer Hospital and Institute and implemented based on the Guide for the Care and Use of Laboratory Animals.

Patient consent for publication

Not applicable.

Competing interests

The authors declare that they have no competing interests.

References

1. Mao R, Zong N, Hu Y, Chen Y and Xu Y: Neuronal death mechanisms and therapeutic strategy in ischemic stroke. Neurosci Bull 38: 1229-1247, 2022.
2. Sommer CJ: Ischemic stroke: Experimental models and reality. Acta Neuropathol 133: 245-261, 2017.
3. Wang L, Ren W, Wu Q, Liu T, Wei Y, Ding J, Zhou C, Xu H and Yang S: NLRP3 inflammasome activation: A therapeutic target for cerebral ischemia-reperfusion injury. Front Mol Neurosci 15: 847440, 2022.
4. Gou X, Xu D, Li F, Hou K, Fang W and Li Y: Pyroptosis in stroke-new insights into disease mechanisms and therapeutic strategies. J Physiol Biochem 77: 511-529, 2021.
5. Duan WL, Wang XJ, Ma YP, Sheng ZM, Dong H, Zhang LY, Zhang BG and He MT: Therapeutic strategies targeting the NLRP3-mediated inflammatory response and pyroptosis in cerebral ischemia/reperfusion injury (Review). Mol Med Rep 29: 46, 2024.
6. Kao TK, Ou YC, Liao SL, Chen WY, Wang CC, Chen SY, Chiang AN and Chen CJ: Opioids modulate post-ischemic progression in a rat model of stroke. Neurochem Int 52: 1256-1265, 2008.
7. Crowley MG, Liska MG, Lippert T, Corey S and Borlongan CV: Utilizing delta opioid receptors and peptides for cytoprotection: implications in stroke and other neurological disorders. CNS Neurol Disord Drug Targets 16: 414-424, 2017.
8. Grant Liska M, Crowley MG, Lippert T, Corey S and Borlongan CV: Delta opioid receptor and peptide: A dynamic therapy for stroke and other neurological disorders. Handb Exp Pharmacol 247: 277-299, 2018.
9. Vaidya B, Sifat AE, Karamyan VT and Abbruscato TJ: The neuroprotective role of the brain opioid system in stroke injury. Drug Discov Today 23: 1385-1395, 2018.
10. Murray A and Hagen NA: Hydromorphone. J Pain Symptom Manage 29 (5 Suppl): S57-S66, 2005.
11. Kim YS, Kim WY, Kim YH, Yoo JW and Min TJ: The protective effect of hydromorphone to ischemia in rat glial cells. Springerplus 5: 610, 2016.
12. Xie W, Xie W, Kang Z, Jiang C and Liu N: Hydromorphone protects CA1 neurons by activating mTOR pathway. Neurosci Lett 687: 49-54, 2018.
13. Zhang J, Li J, An Z and Qi J: Hydromorphone mitigates cardiopulmonary bypass-induced acute lung injury by repressing pyroptosis of alveolar macrophages. Shock 60: 92-99, 2023.
14. Zhang Y, Li X, Qiao S, Yang D, Li Z, Xu J, Li W, Su L and Liu W: Occludin degradation makes brain microvascular endothelial cells more vulnerable to reperfusion injury in vitro. J Neurochem 156: 352-366, 2021.
15. Long J, Sun Y, Liu S, Yang S, Chen C, Zhang Z, Chu S, Yang Y, Pei G, Lin M, *et al*: Targeting pyroptosis as a preventive and therapeutic approach for stroke. Cell Death Discov 9: 155, 2023.

16. Ren X, Wang Z and Guo C: MiR-195-5p ameliorates cerebral ischemia-reperfusion injury by regulating the PTEN-AKT signaling pathway. Neuropsychiatr Dis Treat 17: 1231-1242, 2021.
17. Forouzanfar F, Shojapour M, Asgharzade S and Amini E: Causes and consequences of MicroRNA dysregulation following cerebral ischemia-reperfusion injury. CNS Neurol Disord Drug Targets 18: 212-221, 2019.
18. Zhu F, Luo E, Yi F, Xiong J, Huang C and Li R: LncRNA ITSN1-2 knockdown inhibits OGD/R-induced inflammation and apoptosis in mouse hippocampal neurons via sponging miR-195-5p. Neuroreport 32: 1325-1334, 2021.
19. He KX, Xu L, Ning JZ and Cheng F: MiR-195-5p is involved in testicular ischemia/reperfusion injury by directly targeting PELP1 and regulating spermatogonia pyroptosis. Int Immunopharmacol 121: 110427, 2023.
20. Gao L and Zhang X: Propofol enhances the lethality of cisplatin on liver cancer cells by up-regulating miR-195-5p. Tissue Cell 74: 101680, 2022.
21. Liang E, Xiao S, Zhao C, Zhang Y and Fu G: M6A modification promotes blood-brain barrier breakdown during cerebral ischemia/reperfusion injury through increasing matrix metalloproteinase 3 expression. Heliyon 9: e16905, 2023.
22. Jiang X, Liu B, Nie Z, Duan L, Xiong Q, Jin Z, Yang C and Chen Y: The role of m6A modification in the biological functions and diseases. Signal Transduct Target Ther 6: 74, 2021.
23. Jia K, Xia W, Su Q, Yang S, Zhang Y, Ni X, Su Z and Meng D: RNA methylation pattern and immune microenvironment characteristics mediated by m6A regulator in ischemic stroke. Front Genet 14: 1148510, 2023.
24. Qin Y, Wu S, Zhang F, Zhou X, You C and Tan F: N6-methyladenosine methylation regulator RBM15 promotes the progression of diabetic nephropathy by regulating cell proliferation, inflammation, oxidative stress, and pyroptosis through activating the AGE-RAGE pathway. Environ Toxicol 38: 2772-2782, 2023.
25. Jones-Bolin S: Guidelines for the care and use of laboratory animals in biomedical research. Curr Protoc Pharmacol Appendix 4: Appendix 4B, 2012.
26. Li JH, Liu S, Zhou H, Qu LH and Yang JH: starBase v2.0: Decoding miRNA-ceRNA, miRNA-ncRNA and protein-RNA interaction networks from large-scale CLIP-Seq data. Nucleic Acids Res 42 (Database Issue): D92-D97, 2014.
27. Zhou Y, Zeng P, Li YH, Zhang Z and Cui Q: SRAMP: Prediction of mammalian N6-methyladenosine (m6A) sites based on sequence-derived features. Nucleic Acids Res 44: e91, 2016.
28. Rauluseviciute I, Riudavets-Puig R, Blanc-Mathieu R, Castro-Mondragon JA, Ferenc K, Kumar V, Lemma RB, Lucas J, Chèneby J, Baranasic D, *et al*: JASPAR 2024: 20th anniversary of the open-access database of transcription factor binding profiles. Nucleic Acids Res 52 (D1): D174-D182, 2024.
29. Liu C, Gao Q, Dong J and Cai H: Usf2 deficiency promotes autophagy to alleviate cerebral ischemia-reperfusion injury through suppressing YTHDF1-m6A-mediated Cdc25A translation. Mol Neurobiol 61: 2556-2568, 2024.
30. Zhong Y, Gu L, Ye Y, Zhu H, Pu B, Wang J, Li Y, Qiu S, Xiong X and Jian Z: JAK2/STAT3 axis intermediates microglia/macrophage polarization during cerebral ischemia/reperfusion injury. Neuroscience 496: 119-128, 2022.
31. Guo P, Jin Z, Wu H, Li X, Ke J, Zhang Z and Zhao Q: Effects of irisin on the dysfunction of blood-brain barrier in rats after focal cerebral ischemia/reperfusion. Brain Behav 9: e01425, 2019.
32. Yang Y, Hu F, Yang G and Meng Q: Lack of sphingomyelin synthase 2 reduces cerebral ischemia/reperfusion injury by inhibiting microglial inflammation in mice. Exp Ther Med 20: 241, 2020.
33. Cai L, Yao ZY, Yang L, Xu XH, Luo M, Dong MM and Zhou GP: Mechanism of electroacupuncture against cerebral ischemia-reperfusion injury: reducing inflammatory response and cell pyroptosis by inhibiting NLRP3 and caspase-1. Front Mol Neurosci 15: 822088, 2022.
34. Diaz-Ruiz A, Vacio-Adame P, Monroy-Noyola A, Mendez-Armenta M, Ortiz-Plata A, Montes S and Rios C: Metallothionein-II inhibits lipid peroxidation and improves functional recovery after transient brain ischemia and reperfusion in rats. Oxid Med Cell Longev 2014: 436429, 2014.
35. Zhou J, Wu JS, Yan Y, Li J, Ni T, Shao W, Mei JH, Xiong WZ and Wu H: MiR-199a modulates autophagy and inflammation in rats with cerebral infarction via regulating mTOR expression. Eur Rev Med Pharmacol Sci 24: 6338-6345, 2020.
36. Rong W, Yang L, Li CY, Wu XT, Zhou ZD, Zhu WL and Yan Y: MiR-29 inhibits neuronal apoptosis in rats with cerebral infarction through regulating Akt signaling pathway. Eur Rev Med Pharmacol Sci 24: 843-850, 2020.
37. Longa EZ, Weinstein PR, Carlson S and Cummins R: Reversible middle cerebral artery occlusion without craniectomy in rats. Stroke 20: 84-91, 1989.
38. Wang P, Cui Y, Ren Q, Yan B, Zhao Y, Yu P, Gao G, Shi H, Chang S and Chang YZ: Mitochondrial ferritin attenuates cerebral ischaemia/reperfusion injury by inhibiting ferroptosis. Cell Death Dis 12: 447, 2021.
39. Hu Y, Ye C, Cheng S and Chen J: Propofol downregulates lncRNA MALAT1 to alleviate cerebral ischemia-reperfusion injury. Inflammation 44: 2580-2591, 2021.
40. Guo Y, Yang JH, He Y, Zhou HF, Wang Y, Ding ZS, Jin B and Wan HT: Protocatechuic aldehyde prevents ischemic injury by attenuating brain microvascular endothelial cell pyroptosis via lncRNA Xist. Phytomedicine 94: 153849, 2022.
41. Kong LY, Zhu SY, Si MY, Xu XH, Yu JJ, Zhong WX, Sang CP, Rao DY, Xie FC, Liu ZY and Tang ZX: TAK-242 protects against oxygen-glucose deprivation and reoxygenation-induced injury in brain microvascular endothelial cells and alters the expression pattern of lncRNAs. J Thorac Dis 15: 2571-2584, 2023.
42. Han C, Zhai L, Shen H, Wang J and Guan Q: Advanced glycation end-products (AGEs) promote endothelial cell pyroptosis under cerebral ischemia and hypoxia via HIF-1α-RAGE-NLRP3. Mol Neurobiol 60: 2355-2366, 2023.
43. Kong LY, Liang MY, Liu JP, Lai P, Ye JS, Zhang ZX, Du ZM, Yu JJ, Gu L, Xie FC, *et al*: Mesenchymal stem cell-derived exosomes rescue oxygen-glucose deprivation-induced injury in endothelial cells. Curr Neurovasc Res 17: 155-163, 2020.
44. Zhao B, Fei Y, Zhu J, Yin Q, Fang W and Li Y: PAF receptor inhibition attenuates neuronal pyroptosis in cerebral ischemia/reperfusion injury. Mol Neurobiol 58: 6520-6539, 2021.
45. Waithe OY, Anderson A, Muthusamy S, Seplovich GM and Tharakan B: Homocysteine induces brain and retinal microvascular endothelial cell barrier damage and hyperpermeability via NLRP3 inflammasome pathway differentially. Microcirculation 32: e70019, 2025.
46. Wang J, Xu Z, Chen X, Li Y, Chen C, Wang C, Zhu J, Wang Z, Chen W, Xiao Z and Xu R: MicroRNA-182-5p attenuates cerebral ischemia-reperfusion injury by targeting Toll-like receptor 4. Biochem Biophys Res Commun 505: 677-684, 2018.
47. Liu C, Xu X, Huang C, Zhang L, Shang D, Cai W and Wang Y: Circ_002664/miR-182-5p/Herpud1 pathway importantly contributes to OGD/R-induced neuronal cell apoptosis. Mol Cell Probes 53: 101585, 2020.
48. Liu C, Sui H, Li Z, Sun Z, Li C, Chen G, Ma Z, Cao H and Xi H: THBS1 in macrophage-derived exosomes exacerbates cerebral ischemia-reperfusion injury by inducing ferroptosis in endothelial cells. J Neuroinflammation 22: 48, 2025.
49. Dimopoulos C, Damaskos C, Papadakis M, Garmpis N, Kontzoglou K, Perrea D, Moraitis S, Daskalopoulou A, Papaspirou I, Georgopoulos S and Nikiteas N: Expression of S100B protein in ischemia/reperfusion-induced brain injury after cyclosporine therapy: A biochemical serum marker with prognostic value? Med Sci Monit 25: 1637-1644, 2019.
50. Livak KJ and Schmittgen TD: Analysis of relative gene expression data using real-time quantitative PCR and the 2(-Delta Delta C(T)) method. Methods 25: 402-408, 2001.
51. Jiang Z, Shi L, Huang H, Lei D, Lou L, Jin Y, Sun J and Wang L: Downregulated FTO promotes MicroRNA-155-mediated inflammatory response in cerebral ischemia/reperfusion injury. Neuroscience 526: 305-313, 2023.
52. Wang X, Tian L, Li Y, Wang J, Yan B, Yang L, Li Q, Zhao R, Liu M, Wang P and Sun Y: RBM15 facilitates laryngeal squamous cell carcinoma progression by regulating TMBIM6 stability through IGF2BP3 dependent. J Exp Clin Cancer Res 40: 80, 2021.
53. Kiyosawa N, Watanabe K, Toyama K and Ishizuka H: Circulating miRNA signature as a potential biomarker for the prediction of analgesic efficacy of hydromorphone. Int J Mol Sci 20: 1665, 2019.
54. Mazer-Amirshahi M, Motov S and Nelson LS: Hydromorphone use for acute pain: Misconceptions, controversies, and risks. J Opioid Manag 14: 61-71, 2018.
55. Pickering G, Kotlinska-Lemieszek A, Krcevski Skvarc N, O'Mahony D, Monacelli F, Knaggs R, Morel V and Kocot-Kepska M: Pharmacological pain treatment in older persons. Drugs Aging 41: 959-976, 2024.

56. Liu L, Xu M, Wang J, Hu Y and Huang Z: Research progress of hydromorphone in clinical application. Physiol Res 74: 41-48, 2025.
57. Wang J, Wang N, Zhou H and Wang Y: Effect of preoperative hydromorphone in patients undergoing laparoscopic radical gastrectomy. A double-blind, randomized and controlled trial. Saudi Med J 39: 1023-1027, 2018.
58. Gao L, Dong Q, Song Z, Shen F, Shi J and Li Y: NLRP3 inflammasome: A promising target in ischemic stroke. Inflamm Res 66: 17-24, 2017.
59. Ghafouri-Fard S, Shoorei H and Taheri M: Non-coding RNAs participate in the ischemia-reperfusion injury. Biomed Pharmacother 129: 110419, 2020.
60. Corre S and Galibert MD: Upstream stimulating factors: Highly versatile stress-responsive transcription factors. Pigment Cell Res 18: 337-348, 2005.
61. Fujimi TJ and Aruga J: Upstream stimulatory factors, USF1 and USF2 are differentially expressed during Xenopus embryonic development. Gene Expr Patterns 8: 376-381, 2008.
62. Xie Y, Li X, Deng W, Nan N, Zou H, Gong L, Chen M, Yu J, Chen P, Cui D and Zhang F: Knockdown of USF2 inhibits pyroptosis of podocytes and attenuates kidney injury in lupus nephritis. J Mol Histoln 54: 313-327, 2023.